Impaired plasticity of intrinsic excitability in the dentate gyrus alters spike transfer in a mouse model of Alzheimer's disease

Nan Jiang, Dario Cupolillo, Noelle Grosjean, Emeline Muller, Séverine Deforges, Christophe Mulle, Thierry Amédée

Neurobiology of Disease 154 (2021) 105345

Contents lists available at ScienceDirect

Neurobiology of Disease

journal homepage: www.elsevier.com/locate/ynbdi

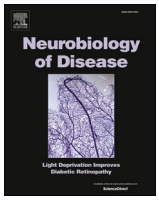

Impaired plasticity of intrinsic excitability in the *dentate gyrus* alters spike transfer in a mouse model of Alzheimer's disease

Nan Jiang, Dario Cupolillo, Noelle Grosjean, Emeline Muller, Séverine Deforges, Christophe Mulle, Thierry Amédée *

Univ. Bordeaux, CNRS, INSERM, Bordeaux Imaging Center, BIC, UMS 3420, US 4, F-33000 Bordeaux, France

ARTICLE INFO

Keywords:
Alzheimer's disease
Dentate gyrus
Intrinsic excitability
Perforant pathway
Synaptic plasticity
Hippocampus
Glial cells
Neuroinflammation

ABSTRACT

Alzheimer's disease (AD) is a progressive neurodegenerative disease characterized by cognitive decline related to deficits in synaptic transmission and plasticity. We report in APP/PS1 mice, a double transgenic mouse model of AD, that females displayed an early burden of Aβ plaques load in the *stratum moleculare* of the *dentate gyrus* (DG) together with prominent neuroinflammatory activation of astrocytes and microglia. Robust deficits in hippocampus-dependent memory tasks were observed in APP/PS1 female mice as early as 3 months of age. We then studied the functional properties of the lateral perforant path (LPP) to DG granule cells. Remarkably DG granule cells displayed higher intrinsic excitability in APP/PS1 female mice. We showed that the long term potentiation of population spike amplitude induced by high frequency stimulation (HFS) at LPP-DG granule cells synapse is impaired in APP/PS1 female mice. HFS induced plasticity of intrinsic excitability in DG granule cells without inducing noticeable modification of synaptic strength. Furthermore, the enhanced intrinsic excitability was potentiated to a greater extent in APP/PS1 as compared to control mice following HFS. Our study shows that changes in the intrinsic excitability of DG granule cells in AD contribute to the dysfunctional transfer of information from the entorhinal cortex to the hippocampus.

1. Introduction

Alzheimer's disease (AD) is a devastating neurodegenerative disease that accounts for more than 70% of dementia in the elderly population worldwide (in "2018 Alzheimer's disease fact and figures", Alzheimer's Association Report, 2018) but despite considerable research efforts, there is still no cure or even effective treatments to alleviate its symptoms.

AD is characterized by two major histopathological hallmarks, Aβ plaques mainly in the cortex and the hippocampus and intraneuronal accumulation of neurofibrillary tangles of hyperphosphorylated Tau (Querfurth and LaFerla, 2010). At late stages, AD brains exhibit profound structural changes such as shrinkage of the cortex and severe atrophy of the hippocampus. These cellular events are associated with prominent neuroinflammation and a large body of evidence has reported that soluble Aβ and numerous molecules produced by inflamed glial cells contribute to the pathophysiology of AD (Akiyama et al., 2000; Heneka and O'Banion, 2007; Heneka et al., 2015; Sarlus and Heneka, 2017).

The hippocampus is characterized by an excitatory tri-synaptic pathway formed by the perforant pathway to *dentate gyrus* (DG) granule cells synapse (PP-DG synapse) followed by the projection of DG granule cells axons (mossy fiber, Mf) to CA3 pyramidal neurons (Mf-CA3 synapse), which in turn project to CA1 pyramidal neurons *via* the Schaffer collateral pathway (SC-CA1 synapse). Entorhinal Cortex - Hippocampus network is one of the first brain regions to be heavily targeted by AD (Stranahan and Mattson, 2010; Criscuolo et al., 2017) and it is acknowledged that alterations of synaptic/dendritic properties of the hippocampus underlie memory deficits in early AD (Penzes et al., 2011). Thus hippocampal synaptic transmission and plasticity have been extensively studied on different transgenic mouse model of the pathology (Marchetti and Marie, 2011) over the last two decades. From this corpus of data has emerged the general picture of an alteration of synaptic circuits at the early stage of the disease (Selkoe, 2002; Spires-Jones and Hyman, 2014; Forner et al., 2017). However while the vast majority of the studies have been focused on the alterations of different

* Corresponding author at: Université de Bordeaux, IINS - UMR 5297 CNRS - Centre Broca Nouvelle Aquitaine, 146 rue Léo Saignat, CS 61292 Case 130, 33076 Bordeaux Cedex, France.
E-mail address: thierry.amedee@u-bordeaux.fr (T. Amédée).

https://doi.org/10.1016/j.nbd.2021.105345
Received 22 January 2021; Received in revised form 16 March 2021; Accepted 19 March 2021
Available online 22 March 2021

forms of hippocampal synaptic plasticity, the presumed alterations in intrinsic neuronal properties, the other key actor of information processing (Daoudal and Debanne, 2003) has so far been poorly taken into account in the context of the pathology.

The *dentate gyrus* (DG) is the main gateway for entorhinal cortex inputs to hippocampus. As such, the plasticity of synaptic transmission within the DG has long been considered to play a crucial role in the processing of cortical information entering the hippocampus. However, DG granule cells are relatively reluctant to Hebbian-type of synaptic plasticity in response to classical induction protocols (Schmidt-Hieber et al., 2004; Lopez-Rojas et al., 2016) whereas they display high plasticity of intrinsic excitability (Lopez-Rojas et al., 2016). This non-synaptic form of plasticity may be essential to control the transfer of information in the DG since the generation of action potentials, which depends not only on excitatory synaptic drive but also on intrinsic excitability, is the main determinant of neuronal activity.

We therefore decided to study the plasticity of intrinsic excitability of DG granule cells in WT female mice and to investigate whether and how this plasticity was affected by the pathology in APP/PS1 mice. We took advantage of the recapitulation by amyloidogenic mouse models of AD of the higher prevalence and greater AD neuropathology for women over men (Barnes et al., 2005; Sinforiani et al., 2010). APP/PS1 females mice display earlier and higher β amyloid plaque load and earlier deficits in hippocampus-dependent memory tasks compared to age-matched males (Gallagher et al., 2013; Richetin et al., 2017).

We first characterized in APP/PS1 female mice the hippocampal progression of Aβ plaque deposition in relation to the glial neuroinflammatory status and deficits in hippocampus-dependent memory tasks in order to establish an early age at which robust histopathological and behavioral alterations were present. We showed that APP/PS1 female mice at 6 months of age displayed a significant load of Aβ plaques as well as prominent neuroinflammatory activation of astrocytes and microglia in the *stratum moleculare* of the *dentate gyrus*, a region described as being affected early in the spatiotemporal progression of the disease (Hurtado et al., 2010). Early deficits in the contextual fear conditioning and the object location task, two hippocampus-dependent tasks resulting in a robust long lasting memory for a rodent (Phillips and LeDoux, 1992) were also observed.

Having shown that APP/PS1 female mice at the age of 6 months displayed obvious molecular and behavioral alterations, we focused our study on the lateral perforant pathway (LPP), which conveys multimodal sensory informations originated in the entorhinal cortex to the DG (Hunsaker et al., 2007; Deng et al., 2010). We show that APP/PS1 female mice at 6 months of age show an alteration of the plasticity of spike transmission at LPP-synaptic inputs and even more remarkably, that the plasticity of intrinsic excitability of DG granule cells is prominently impacted by the pathology. Our results reveal new mechanisms that may lead to dysfunction in the transfer of information from the entorhinal cortex to the hippocampus and may delineate new routes for improvement and/or therapeutic intervention.

2. Materials and methods

2.1. Ethical approval

Animal anesthesia and euthanasia were carried out in accordance with the Animal Protection of ethical standards and the French legislation concerning animal experimentation and were approved by the University of Bordeaux/CNRS Animal care and Use Committee (authorization #03524). All efforts to improve the animal welfare and to minimize animals suffering were made.

2.2. Animals

The animals used in this study were males and females APPswe695/PS1ΔE9 termed APP/PS1 (Stock number: 005864) obtained from Jackson Laboratory (Bar Harbor, ME, USA) and their wild-type (WT) littermates (C57BL6/J). Briefly, the APP/PS1 mice express a chimeric mouse/human amyloid precursor protein APPswe (mouse APP695 harboring a human Aβ domain and mutations K595N and M596L linked to a Swedish familial AD) and a human presenilin 1 mutated in familial AD (PS1ΔE9; deletion of exon 9). These bigenic mice were created by co-injection of both transgenes allowing for a co-segregation of the transgenes as a single locus (Jankowsky et al., 2004). Mice were generated in our animal facility from double-transgenic APP/PS1 males mated with C57BL/6 J females. Transgenic mice (APP/PS1) and age-matched non-transgenic littermates (WT) were allowed free access to food and water and maintained in a 12 h dark-light cycle. Mice were genotyped and systematically regenotyped after each experiments (Transcriptomics Platform, Neurocentre Magendie, Bordeaux, France). In all experiments, females were used regardless of their estrous cycle.

2.3. Acute hippocampal slices

APP/PS1 and WT female mice at 6 months of age were deeply anesthetized with a mix of ketamine (80 mg/kg; i.p) and xylazine (16 mg/kg; i.p) and then intracardially perfused for 2–3 min with a protective solution at 4 °C containing the following (in mM): 2.5 KCl, 1.25 NaH_2PO_4, 0.5 $CaCl_2$, 7 $MgCl_2$, 20 glucose, 26 $NaHCO_3$, 76 sucrose, 3 pyruvic acid, 5 Na ascorbate, equilibrated with 95% 0_2 and 5% CO_2 (300–310 mOsm). When the solution leaving the heart was free of blood, the mouse was sacrificed by decapitation and the brain was quickly removed from the skull and stored in the same solution. The isolated brain was glued onto the stage of a vibratome (VT 1200S, Leica Microsystems, Nussloch, Germany) and parasagittal hippocampal slices (320 μm) were cut in the protective solution for which sodium chloride was replaced by sucrose, and then incubated at 33 °C for 10–20 min in a resting solution containing the following (in mM): 125 NaCl, 2.5 KCl, 1.25 NaH_2PO_4, 2 $CaCl_2$, 1 $MgCl_2$, 20 glucose, 26 $NaHCO_3$, 5 Na ascorbate equilibrated with 95% 0_2 and 5% CO_2 (300–310 mOsm). The slices were thereafter maintained at room temperature in the same solution until required. Only the dorsal slices were retained in this study as the dorsally located hippocampal segment mediate cognitive operations like spatial navigation, which is critically impaired in mouse models of AD (Bannerman et al., 2014; Strange et al., 2014) whereas functions related to emotions are preferentially taken on by the ventral segment of the hippocampus (Kheirbek et al., 2012).

2.4. Electrophysiological studies on acute hippocampal slices

For recording, the slices were transferred to a recording chamber where they were submerged and perfused with an extracellular recording solution containing the following (in mM): 125 NaCl, 2.5 KCl, 1.35 NaH_2PO_4, 2 $CaCl_2$, 1 $MgCl_2$, 16 glucose, 26 $NaHCO_3$ continuously oxygenated (95% 0_2 and 5% CO_2). The recordings were made at room temperature. Whole-cell patch clamp recordings (3–4 MΩ electrodes, −70 mV holding potential) were made from *dentate gyrus* (DG) granule cells visualized by infrared video-microscopy. Patch clamp electrodes were pulled out from borosilicate glass (GF 150 F-10) and filled with an internal solution containing the following (in mM): 140 $CsCH_3SO_3$, 2 $MgCl_2$, 4 NaCl, 5 phospho-creatine, 2 Na_2ATP, 0.2 EGTA, 10 HEPES, and 0.33 GTP adjusted with CsOH (300 mOsm, pH 7.3). For patch-clamp recordings in current-clamp mode, a K^+-based internal solution containing (in mM) was used: 115 K-gluconate, 10 KCl, 0.2 EGTA, 10 HEPES, 15 phospho-creatine, 4 MgATP and 0.3 NaGTP adjusted with KOH (300–305 mOsm, pH 7.3). Bicuculline (10 μM) was added to the bath to inhibit γ-Aminobutyric acid-A (GABA-A) receptors. Voltage-clamp recordings were performed on DG granule cells identified with a differential interference contrast microscope (Eclipse FN-1, Nikon, Champigny sur Marne, France) equipped with an infrared camera (VX 44, Till Photonics, Gräfelfing, Germany) using an Axopatch-200B amplifier (Axon Instruments, Sunnyvale, CA, USA). Signals were

filtered at 2 kHz and digitized at 5 kHz *via* a DigiData 1322A interface (Axon instruments). In order to check the quality of patch clamp recordings, series resistance (10–20 MΩ) was monitored during the recording using a − 10 mV hyperpolarizing voltage step of 50 ms length occurring at the beginning of each recording and DG granule cells were rejected if more than a 20% change occurred during the experiment. In addition, DG granule cells with a holding current exceeding 250 pA at a holding potential of −70 mV were also rejected. No liquid-junction potential correction was used. Data were collected and analysed using pClamp software 9.2 (Axon Instruments).

Field recordings were obtained from the granular cell layer using glass electrodes (1–2 MΩ) filled with extracellular recording solution. Due to the possibility of crosstalk between mossy cell fibers (MCFs) and the more proximal medial perforant path (MPP) we focused our study on lateral perforant path (LPP) transmission. To selectively stimulate the LPP, a stimulating glass electrode (1–2 μm tip diameter) filled with extracellular recording solution was placed in the outer molecular layer of the DG (>100 μm away from the granule cell layer) and as close as possible to the hippocampal fissure, which is located 180–250 μm away from the granule cell layer (Allen Brain Atlas©). In addition to the location of the stimulating electrode, we characterized the LPP by its ability to exhibit paired-pulse facilitation whereas the MPP does not (Fig. 2B). Signals were recorded using an Axopatch-200B amplifier (Axon Instruments, Sunnyvale, CA, USA), filtered at 20 kHz and digitally sampled at 50 kHz. All experiments were performed in the presence of bicuculline (10 μM) to block GABA-A receptors. GABA-B receptors, which are expressed by both axonal terminal and dendritic compartment of DG granule cells, were not blocked as these receptors primarily exert disinhibition on DG granule cells due to the reduction of GABA release from hilar interneurons (Foster et al., 2013). Input-output curves were recorded by varying stimulation strength from 0 to 300 μA in 50 μA intervals. For subsequent experiments on basal transmission and population spike recordings, the stimulus strength was set to a level that produced about 30–35% of the maximal responses. Proper stimulating electrode location was controled by applying a paired-pulse protocol to the recorded population spike. The protocol for population spike potentiation consisted of a high-frequency stimulation (HFS) of 3 bursts of 100 stimuli at 100 Hz with a 10 s interburst interval. In patch clamp experiments, HFS was paired with a postsynaptic depolarization at 0 mV in order to facilitate the removal of the magnesium block of NMDA receptors. E-S curve, which relates EPSP slopes to the associated action potential (AP) firing probability, was generated by measuring slopes during the first 2 ms (reflecting mainly the fast component of AMPA-receptor synaptic transmission) and sorted in 0.5 mV/ms bins to the associated AP firing probability. The AP firing probability was calculated for each bin and the EC_{50} value (the value of the EPSP-slope that elicits an AP with 50% of probability) was calculated in each cell. EPSP amplitude/slope ratio histograms before and after HFS were generated as follows: at the start of the experiment, for each cell the amplitude of sub-threshold EPSPs (*i.e.* not triggering APs) was measured in current-clamp mode (the membrane potential was set to around −70 mV), and plotted *vs* the EPSP slope. Then a linear regression was fitted yielding a slope value. The cell was rejected if the goodness of fit, $S_{y.x}$, which quantifies the scatter of the data points around the best fit line was <1.5. After this, the cell was switched to voltage-clamp mode and held at −70 mV. A baseline was recorded for 5 min and then the HFS protocol was applied followed by a period of 20 min. Then the cell was returned back to current-clamp mode (set around - 70 mV) and a new EPSP amplitude/slope ratio histogram was generated.

2.5. Immunohistological staining and analysis

WT and APP/PS1 male and female mice at 3, 6 and 9 months of age were anesthetized with intraperitoneal administration of pentobarbital (50 mg/kg body weight) and were fixed by transcardial perfusion with buffered saline and 50 ml of 4% paraformaldehyde (PFA). The brains were removed, postfixed in 4% PFA overnight and cut into 40 μm-thick frontal sections on a vibratome. The sections were collected into PBS 0.1 M and stored at +4 °C until the staining protocol. After a thorough wash in TBST (Tris Buffer Sodium: 0.0384 M Trisma Base −0.1263 M NaCl pH: 7.4 + 0.1% Tween 20), free-floating sections were incubated with TBST - 10% Normal Goat Serum - 0.3% Triton X-100, for 1 h at room temperature. Then the sections were incubated with primary antibody in TBST - 3.5% Normal Donkey Serum overnight at 4 °C (chicken anti - glial fibrillary acidic protein (GFAP): 1/1000 USBiologicals; rabbit anti - ionized calcium-binding adapter molecule Iba-1: 1/5000 Wako. Aβ plaques were stained either using Methoxy-X04 (Congo red derivative, 50 μM, Tocris) or mouse anti-$Aß_{1–16}$: 1/150 (Millipore). After washes in TBST, sections were incubated with secondary antibodies for 1 h (Goat anti-chicken Alexa 647, anti-mouse Alexa 555 and anti-rabbit Alexa 488: 1/500, Invitrogen). The slices were finally washed and mounted in mounting medium (Fluoromount + DAPI, SouthernBiotech). The slices were imaged using the up-right widefield microscope Leica DM5000 (Leica Microsystems, Nanterre, France) using objectives HC PL Fluotar 20× NA 0.5. Fluorescence excitation was performed by a LED SOLA Light (Lumencor, Beaverton, USA). Images were obtained by the resolutive cameras CoolSnap HQ2 (Photometrics, Tucson, USA) and a cooled QICAM (QImaging, Surrey, Canada). A galvanometric stage (Leica Microsystems) allowed the z stack reconstructions. The mosaics were created using a motorized stage Scan (Märzhäuser, Wetzlar, Germany). This system was controlled by MetaMorph software (Molecular Devices, Sunnyvale, USA). Analyses were performed with Image J software (National Institutes of Health, New York, USA) on the maximum intensity fluorescence projections of the 3D mosaics. The images were then calibrated and processed as 8-bits grayscale images (0–255) by Image J software. A high manual threshold was applied to Aβ plaques and to GFAP positive cells and Iba-1 positive cells to remove irrelevant signals. The manual threshold was adjusted to count only dense core Aβ plaques. Between 8 and 10 measurements from 5 mice were acquired per genotype and per stained protein.

2.6. Contextual fear conditioning (CFC)

Mice were housed individually. Prior to the test, mice were handled 2 min per day during 5 days. At day 0, single-trial contextual fear conditioning was performed by placing mice into a conditioning chamber where they were allowed to explore for 150 s after which they received a mild electric footshock (2 s, 0.7 mA) and were removed 28 s after the shock. The conditioning chamber was housed in a sound attenuated box with the four interior walls wearing a checkerboard pattern. The conditioning cage (17 cm wide, 17 cm deep and 25 cm high) was made of clear plexiglas and the floor consisted of a shock grid. Between each animal the cage was cleaned with 70% ethanol solution. At day 1, mice were reexposed to the conditioning chamber during 180 s. The cage was cleaned with 1% acetic acid between each mouse. Contextual fear memory retention was studied by measuring the freezing response in the conditioning chamber. The chamber was filmed with a ceiling-mounted Charge Coupled Device (CCD) camera connected to a Windows computer. Images of the apparatus and the mouse were captured and analysed by the application software program (Any-Maze, Ugo Basile, Gemonio, Italy). The frame rate was set at 15 fps. Freezing behavior, defined as behavioral immobility except for movements necessary for breathing, was continuously recorded for each mouse and detected with the help of the software. The rationale of freezing detection is based on the finding by the software of a sequence of images in which there is no movement before it will actually score the mouse as “freezing”. It means that the moment the software concludes that the mouse is freezing will always be a short time after the freezing actually began. To be able to distinguish between freezing and immobility, in this software the freezing detection is completely unrelated to the tracking of the mouse. The minimum freeze duration was set at 400 ms. To objectivate the accuracy of freezing detection by the software, in a first set of

experiments, the automatic freezing detection time was compared to scoring of it by an observer blind to the genotype of the mice. As both methods gave similar results, in the rest of the study automatic detection was used.

2.7. Object Location Task (OLT)

Prior to the test, mice were handled 2 min per day during 5 days and habituated to the openfield (45 cm wide, 45 cm deep and 40 cm high) the day before the experiment during 20 min, in the absence of objects. The total covered distance was measured by video-tracking (Noldus-Ethovision, Nantes, France). On the day of the test, mice were first placed for 10 min (habituation phase) in the arena where two identical blue plastic bricks were located 15 cm away from the walls in adjacent quadrants (A and C or B and D). Brick exploration was defined as exploration with the nose directing towards it within 2 cm. The absence of preference with one of the two bricks was checked during the habituation phase. After a delay of 30 min, mice were reexposed to the arena in which one of the two bricks was moved (for example from quadrant B to quadrant A or from quadrant D to quadrant C) in order to create a new spatial combination and mice were allowed to explore for again 10 min. The time spent exploring the bricks in the novel and familiar locations was measured during the first 5 min as mice have tendancy to lose novelty detection behavior after few minutes (Cès et al., 2018). The discrimination ratio was determined by the percentage of the time spent exploring the displaced brick over the time spent exploring both bricks.

2.8. Experimental design and statistical analysis

In order to minimize biases as much as possible, the experimenters were kept blind to the genotype of the mice until the analysis was completed. Values are presented as mean ± SEM (standard error of mean) of n experiments. Statistical analyses were performed with Prism 7.0 (GraphPad Software, La Jolla, CA, USA). First the normality of data set was tested using the D'Agostino-Pearson omnibus normality test. If data was normally distributed, a Student's *t* - test for 2 groups and a two way ANOVA with Bonferonni's test for more than two groups were used for statistical comparison. The *P*-values given are two-tailed and were considered significant if $p < 0.05$. One-proportion *Z*-test was used for proportion analysis (Fig. 3A).

2.9. Drugs

Bicuculline, D-2-amino-5-phosphonopentanoate (D-AP5) and Methoxy-X04 were obtained from Tocris, TTX and D-serine from Sigma-Aldrich, NBQX from HelloBio. Stock solutions using appropriate solvent (DMSO for bicuculline, D-AP5 and Methoxy-X04 and acetic acid for TTX) were made and diluted with aCSF just before the application.

3. Results

3.1. Histopathological and behavioral alterations in APP/PS1 female mice

In order to set an age at which a significant deposit of hippocampal Aβ plaques occurred, we study the time course of the expression of hippocampal Aβ plaques in APP/PS1 female mice at 3, 6 and 9 months of age (Fig. 1). While no plaques were detectable at 3 months of age, numerous plaques were visible at 6 months of age and there was a high load at 9 months of age (Fig. 1A). These results are in good agreement with earlier findings reporting an early and progressive Aβ deposition in APP/PS1 mice (Jankowsky et al., 2004; Garcia-Alloza et al., 2006). Remarkably at 6 and 9 months of age, Aβ plaques (red signal) were not uniformely distributed throughout the hippocampus but were clearly concentrated in the *stratum moleculare* (delineated by the white dotted-line) of the DG (Fig. 1A). At higher magnification (Fig. 1B), Aβ plaques were formed by a dense amyloid core (anti-$A\beta_{1-16}$, white signal) surrounded by a spider web of microglia (Iba-1, green signal). Activated astrocytes (GFAP, red signal) were located in the vicinity. Aβ plaques were counted in the whole hippocampus and in the *stratum moleculare* (DG area) obtained from 5 mice for both genotype. There was a clear progressive increase in the number of Aβ plaques during the course of the pathology (Fig. 1C) for both the whole hippocampus (3 months-old: 5.0 ± 1.7, $n = 20$; 6 months-old: 31.1 ± 3.0, $n = 30$; 9 months-old: 59.8 ± 4.2, $n = 17$, *** $p < 0.001$) and the DG area (3 months-old: 1.9 ± 0.7, $n = 29$; 6 months-old: 8.5 ± 0.8, $n = 56$; 9 months-old: 21.5 ± 2.9, $n = 29$, *** $p < 0.001$).

The neuroinflammatory activation of glial cells is well acknowledged as hallmarks of disease progression (for review see Heneka and O'Banion, 2007; Heneka et al., 2015; Sarlus and Heneka, 2017). To illustrate this in our mouse model, we performed double immunostaining of astrocytes (GFAP, red signal) and microglia (Iba-1, green signal) and compared the pattern of activation between WT and APP/PS1 female mice at 6 months of age (Fig. 1D; Fig. 1E). While, astrocytes showed elongated bodies with long and fine processes in WT mice, they showed rounded cell bodies with shortened and enlarged processes, a morphological hallmark of activated astrocytes (Wilhelmsson et al., 2006; for review see Schiweck et al., 2018) in APP/PS1 mice (Fig. 1D). Microglia also displayed a typical phenotype of reactive cells (Nimmerjahn et al., 2005) shifting from a quiescent morphology with small somas densely arborised with very fine processes in WT mice to an activated status with a prominent enlargement of cell bodies with shortened and thickened processes in APP/PS1 mice (Fig. 1E).

Collectively, these data are unambiguous evidence that Aβ plaques deposition accompanied by hypertrophic astrocytes and amoeboid microglia, all recognized as neuroinflammatory furnaces, starts after 3 months of age in APP/PS1 female and is robust at 6 months of age. Our findings are consistent with numerous reports describing in the APP/PS1 mouse model the progressive onset of amyloid pathology in the form of Aβ plaques deposits starting around 4–6 months of age (for review see Marchetti and Marie, 2011) and extend those of Richetin et al. (2017) reporting the presence of abundant hypertrophic astrocytes in the DG of older APP/PS1 female mice (7–9 months of age).

Hippocampal-dependent memory was tested in APP/PS1 female mice at 3, 4 and 6 months of age and their age-matched WT littermates using two different one-trial behavioral paradigm, *i.e.* contextual fear conditioning (CFC) and object location task (OLT). CFC is a hippocampus-dependent task, which results in a robust long lasting memory for a rodent (Phillips and LeDoux, 1992). Worthy of note, both WT and APP/PS1 mice displayed almost no freezing at 3, 4 and 6 months of age (data not shown) during the 150 s period before the footshock at the time of training (3 months-old: WT: 0.75 ± 0.2%, $n = 11$; APP/PS1: 0.71 ± 0.2%, $n = 11$, $p = 0.911$; 4 months-old: WT: 1.0 ± 0.2%, $n = 14$; APP/PS1: 1.0 ± 0.5%, $n = 9$, $p = 0.997$; 6 months-old: WT: 5.6 ± 1.4%, $n = 15$; APP/PS1: 3.0 ± 0.8%, $n = 10$, $p = 0.186$) evidencing the lack of significant anxiety-related behavior in our experimental conditions. Furthermore, in order to test for possible hyperactivity of APP/PS1 *vs* WT mice, we scored the distance moved (in cm) in an open field session of 20 min at 3, 4 and 6 months of age for both phenotype and found no significant differences (3 months of age, WT: 6476 ± 292, $n = 16$, APP/PS1: 7198 ± 768, $n = 11$, $p = 0.328$; 4 months of age, WT: 3707 ± 539, $n = 11$, APP/PS1: 4984 ± 578, $n = 9$, $p = 0.124$; 6 months of age, WT: 5971 ± 282, $n = 15$, APP/PS1: 7300 ± 700, $n = 12$, $p = 0.069$) (data not shown). As early as 3 months of age, APP/PS1 female mice displayed memory deficits with an impaired CFC (3 months-old: WT: 43.7 ± 4.9%, $n = 11$; APP/PS1: 24.9 ± 5.2%, $n = 11$, *$p < 0.05$, 4 months-old: WT: 37.4 ± 7%, $n = 14$; APP/PS1: 15.2 ± 4.8%, $n = 9$, * $p < 0.05$; 6 months-old: WT: 50.2 ± 5.1%, $n = 15$; APP/PS1: 30.8 ± 6.8%, $n = 10$, *$p < 0.05$) (Fig. 1F).

In a second set of experiments, APP/PS1 females mice of 3, 4 and 6 months of age and their age-matched WT littermates were subjected to

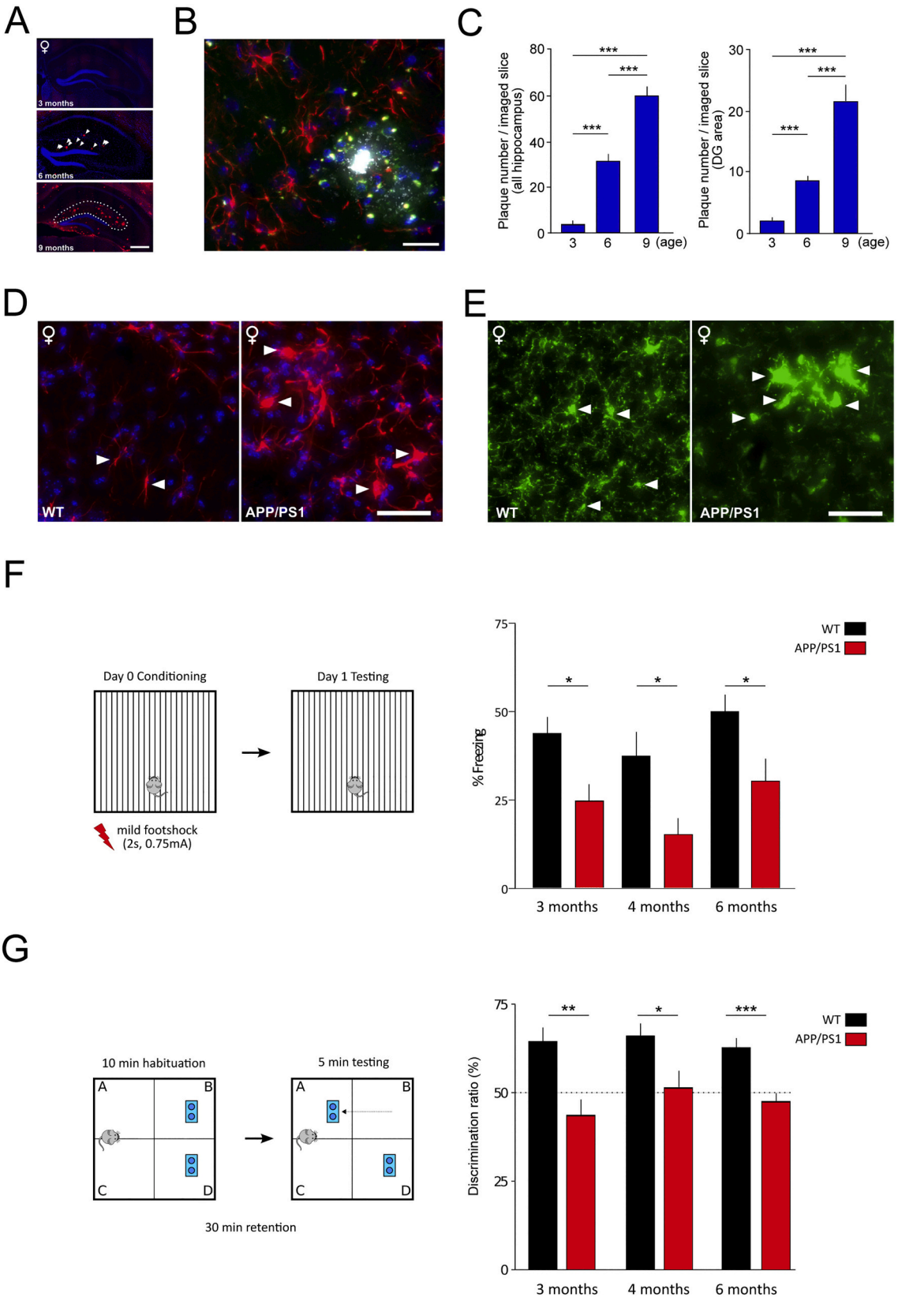

(caption on next page)

Fig. 1. APP/PS1 female mice display molecular and behavioral alterations. A. Representative micrographs of a hippocampus in APP/PS1 female mice at 3, 6 and 9 months of age. Slices were double stained for nuclei with 4′,6-diamidino-2-phenylindole (DAPI, blue signal) and for Aβ plaques with 2,5-Bis(2-(4-hydroxyphenyl) vinyl) anisole (methoxy-X04, red signal). Note the virtual lack of Aβ plaques at 3 months of age and the progressive expression at 6 and 9 months of age (white arrow heads). At 9 months of age, there is an heavy load of Aβ plaques in the hippocampus but more concentrated in the upper molecular layer (delineated by the white dotted-line), *i.e.* the *stratum moleculare* of the DG. Bar scale = 250 μm. B. Representative micrograph of an Aβ plaque formed of an amyloid core (anti-$A\beta_{1-16}$ antibody, white signal) embedded in a spider web of microglia (Iba-1, green signal) and activated astrocytes (GFAP, red signal) in the vicinity in a 9 months old female mouse. Bar scale = 10 μm. C. Bar graphs represent the number of Aβ plaques counted per imaged slice (n) in the whole hippocampus (left panel) and in the DG area as delineated in A (right panel) at 3, 6 and 9 months of age (5 mice). Note the progressive increase of Aβ plaques at each age (female: 3 *vs* 6 months old *** $p < 0.001$; 6 *vs* 9 months old *** $p < 0.001$; 3 *vs* 9 months old *** $p < 0.001$) both in all hippocampus and in the *stratum moleculare* (termed DG area). D. Astrocytic status in the DG area for WT and APP/PS1 female mice at 6 months of age. Note the prominent morphological changes in GFAP positive cells (astrocytes) in APP/PS1 *vs* WT female mice (white arrow head), (DAPI, blue signal). Bar scale = 10 μm. E. Microglial status in the DG area for WT and APP/PS1 female mice at 6 months of age. Note the morphological changes in Iba-1 positive cells (microglia) in APP/PS *vs* WT female mice (white arrow head). Bar scale = 10 μm. F. At day 0, WT and APP/PS1 female mice were placed in a training chamber where they received a mild electric footshock (2 s, 0.75 mA). At day 1, mice were reexposed to the same chamber. Contextual fear memory retention was studied by measuring the freezing response in the chamber and freezing percentage was calculated for each animal (left panel). As early as 3 months of age when compared to WT mice, APP/PS1 female mice show impairment of contextual fear conditioning when reexposed to the training chamber. (* $p < 0.05$). G. APP/PS1 female mice show impaired object location task. Female mice are allowed to explore an open field arena with two identical objects (blue plastic bricks) during the habituation phase (10 min). During the retention phase (30 min) mice were placed back to their home cage. Prior to the test phase, the location of one object is changed and then during the test phase (5 min), the time spent exploring the two objects was assessed (left panel). As early as 3 months of age, APP/PS female mice show impaired object location task (right panel). Discrimination ratio = time spent to explore the displaced object/total time spent to explore both objects. (* $p < 0.05$; ** $p < 0.01$; *** $p < 0.001$).(For interpretation of the references to color in this figure legend, the reader is referred to the web version of this article.)

OLT (Fig. 1G). OLT addresses hippocampus-dependent spatial memory (Ennaceur et al., 1997; Mumby et al., 2002; Haettig et al., 2011), which relies on the mouse's innate preference for novelty. Remarkably this task does not involve the retrieval of an aversive stressful training event, which does not reflect typical day-to-day memories usually affected in the human pathology. Mice that remember the habituation phase will preferentially explore the displaced object (novel location) relative to the nondisplaced one (Fig. 1G left panel). Following the 30 min retention period, WT female mice spent more time exploring the novel location of the object than the familiar one at all age, so that the discrimination ratio was significantly different from 50% (3 months-old: 65.4 ± 4%, $n = 14$, $^{**}p < 0.01$; 4 months-old: 66.3 ± 3.8%, $n = 16$, $^{***}p < 0.001$; 6 months-old: 66.2 ± 3%, $n = 15$, $^{**}p < 0.01$). In contrast and as early as 3 months of age, APP/PS1 females did not explore the novel

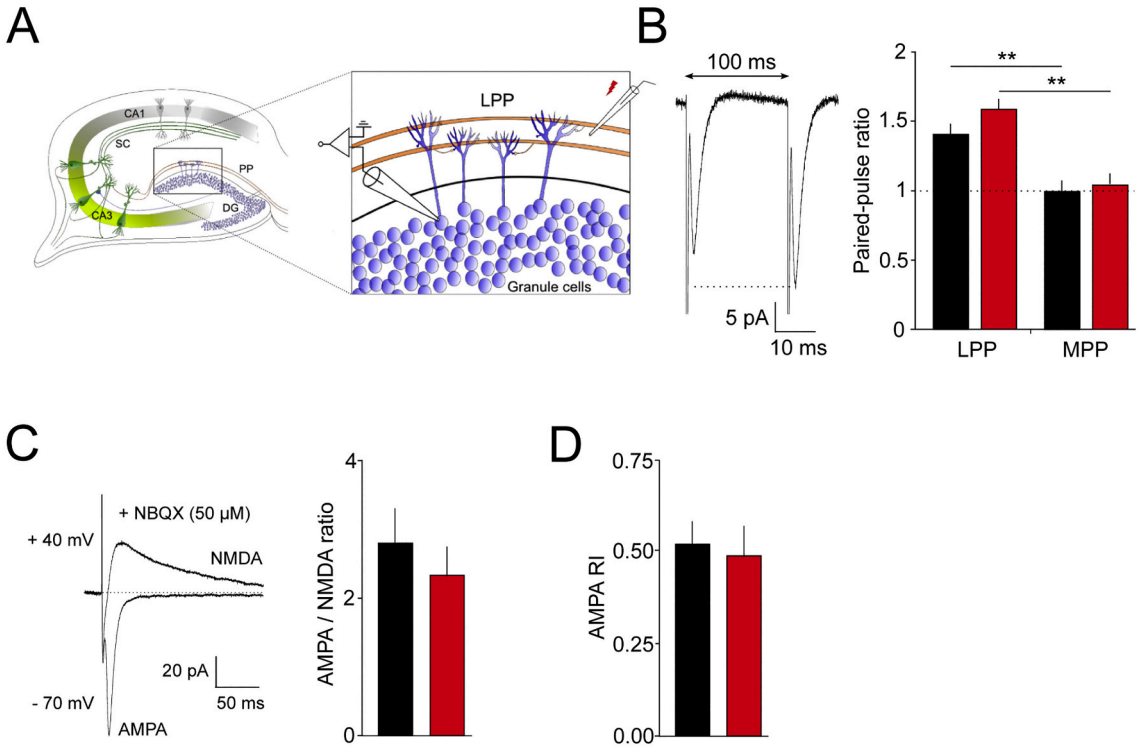

Fig. 2. Electrophysiological characterization of the lateral perforant path (LPP) inputs to the hippocampal *dentate gyrus* (DG). A. Diagram shows the positions of the stimulating electrode (located in the outer DG molecular layer) and of the recording electrode in patch clamp experiments. Please note that the position of the recording electrode is only for illustrative purpose but does not indicate the exact location of recorded DG granule cells. For field recordings, the electrode is placed near the crest of the suprapyramidal blade. B. Electrophysiological dissection of the LPP and medial perforant path (MPP) by paired-pulse experiments in whole-cell patch clamp recordings. DG cells were clamped at −70 mV and the two pulses were separated by 100 ms. For both genotype the paired-pulse ratio was significantly higher for the LPP *vs* MPP (WT: 1.4 ± 0.07, $n = 5$ *vs* 1.01 ± 0.06, $n = 6$, ** $p < 0.01$; APP/PS1: 1.58 ± 0.07, $n = 8$ *vs* 1.03 ± 0.08, $n = 8$, *** $p < 0.001$). C. Representative traces from whole-cell patch clamp experiments showing AMPA-receptor- and NMDA-receptor evoked currents (in the presence of 50 μM NBQX) in DG granule cells. Histograms showing the AMPA to NMDA ratio for WT and APP/PS1 mice (WT:2.82 ± 0.45, $n = 10$; APP/PS1:2.35 ± 0.39, $n = 9$, $p = 0.452$). The AMPA rectification index (AMPA RI) was obtained by dividing the AMPA current amplitude measured at +40 mV by the one measured at −70 mV for WT and APP/PS1 mice (WT:0.51 ± 0.06, $n = 10$; APP/PS1:0.49 ± 0.08, $n = 9$, $p = 0.794$).

location of the object more significantly than the fixed one (3 months-old: 44.2 ± 4.7, $n = 15$, $p = 0.232$; 4 months-old: 51.6 ± 4.9%, $n = 10$, $p = 0.752$; 6 months-old: 47.8 ± 2.3%, $n = 13$, $p = 0.354$) indicating therefore that they were impaired in this task as early as 3 months of age (Fig. 1G right panel). Our data provide clear evidence that starting as early as 3 months of age, APP/PS1 mice were impaired and never explored the new location of the object more than WT mice.

Overall, our results show a progressive increase in Aβ plaques load and neuroinflammatory activation of astrocytes and microglia preferentially located in the *stratum moleculare* of the DG and early deficits in hippocampus-dependent memory tasks. Therefore, based on robust molecular and behavioral alterations, we decided to study the functional properties of the lateral perforant pathway to DG granule cells synapse on APP/PS1 female mice at 6 months of age.

3.2. Functional properties of LPP-DG synapses

Having shown that Aβ plaques were abundant in the *stratum moleculare* of the DG in female mice, we studied the functional properties of synaptic circuitry in the close vicinity, which are PP-DG synapses. Specifically, we focused on the lateral perforant path (LPP) - DG synapse, which processes multimodal sensory information from the entorhinal cortex (Hunsaker et al., 2007; Igarashi et al., 2014). We took great care to differentiate LPP from the medial perforant path (MPP) by placing the stimulating electrode in the outer one-third molecular layer of the DG suprapyramidal blade and the recording electrode either in the DG granule cell layer for patch-clamp recordings as shown in Fig. 2A, or near the crest of the suprapyramidal blade for extracellular field recordings. In this way, we achieved reliable and selective activation of LPP projections to the DG. On the other hand, MPP was selectively activated by positioning the electrode in the middle molecular layer, *i.e.* at a distance <100 μm from the DG granule cell layer. We confirmed the anatomical dissection of the two pathways by using a paired-pulse protocol (McNaughton, 1980; Dahl and Sarvey, 1989; Colino and Malenka, 1993; Petersen et al., 2013), which resulted in facilitation of the second pulse when the LPP is stimulated but no facilitation or even depression of the second pulse when the MPP is stimulated (Fig. 2B). Excitatory post synaptic currents (EPSCs) were recorded in DG granule cells in the whole-cell configuration of the patch clamp technique from a holding potential of −70 mV. Stimuli were delivered at a low intensity that produced EPSCs of approximately 15–20% of the maximum possible amplitude in order to minimize as much as possible current spreading to the adjacent pathway (Petersen et al., 2013). The two pulses were separated by a 100 ms interval between pulses. Both genotypes showed a facilitation for the LPP (WT: 1.4 ± 0.1, $n = 5$; APP/PS1: 1.6 ± 0.1, $n = 8$) but not for the MPP (WT: 1.0 ± 0.1, $n = 6$; APP/PS1: 1.0 ± 0.1, $n = 8$) (Fig. 2B).

Then we investigated if the relative amount of AMPA *vs* NMDA mediated synaptic currents at DG granule cells was affected by the genotype in DG granule cells of APP/PS1 and WT mice (Fig. 2C). AMPA currents were recorded at a holding potential of −70 mV, a potential at which NMDA currents are virtually absent due to the voltage-dependent Mg^{2+} block (Nowak et al., 1984; Mayer et al., 1984). NMDA currents were isolated at a holding potential of +40 mV in the presence of 50 μM NBQX to block AMPA and kainate currents. We found no difference in the AMPA/NMDA ratio between WT (2.82 ± 0.45, $n = 10$) and APP/PS1 mice (2.35 ± 0.39, $n = 9$; $p = 0.452$). In addition, the AMPA rectification index (AMPA RI), a proxy to investigate for possible changes of AMPA receptor properties did not differ significantly between genotypes (WT: 0.51 ± 0.06, $n = 10$; APP/PS1: 0.49 ± 0.08, $n = 9$; $p = 0.794$) suggesting no major alteration in AMPA receptor properties in APP/PS1 mice.

3.3. DG granule cells display higher excitability in APP/PS1 mice

We then characterized the basic intrinsic properties of WT and APP/PS1 DG granule cells, *i.e.* input resistance (R_{in}), total amplitude of AP, amplitude of the overshoot, time to peak of the AP, time to reach the half-maximal amplitude (t_{50}), threshold potential but found no significant differences (Table 1). Only the resting membrane potential was slightly higher for APP/PS1 compared to WT mice (−72.7 ± 0.9 mV, $n = 23$; −75.4 ± 0.7 mV, $n = 15$ respectively, * $p < 0.05$, Table 1). Worthy of note, the minimal current required to trigger APs (I_{thr}) was significantly lower for APP/PS1 compared to WT mice (APP/PS1: 40.3 ± 2 pA, $n = 31$; WT: 56 ± 3.7 pA, $n = 30$, *** $p < 0.001$) (Table 1) indicating a higher intrinsic excitability of APP/PS1 DG granule cells.

DG granule cells in adult mice are constituted of newly born (immature) and mature neurons reflecting their dynamic integration in the DG throughout the life of the organism. These two populations of DG granule cells have been previously described in WT rodents (van Praag et al., 2002; Schmidt-Hieber et al., 2004; Mongiat et al., 2009; Spampanato et al., 2012) and their relative contribution to memory processing such as pattern separation and pattern completion have been investigated (Aimone et al., 2011; Nakashiba et al., 2012). Remarkably, these two populations have different intrinsic properties among which the input resistance (R_{in}) and the firing pattern have been used to discriminate them (Nenov et al., 2015). This led us to wonder whether the intrinsic properties of DG cells were differentially affected by Aβ pathology in APP/PS1 mice. Whole-cell patch clamp recordings were carried out in DG granule cells from 6 months-old WT and APP/PS1 female mice. Fig. 3A shows representative electrotonus and action potentials (APs) in DG granule cells from a WT mouse in response to long (250 ms) injections of 10 pA depolarizing current step increments from 60 pA up to 200 pA in current-clamp mode at a membrane potential close to −70 mV. On the basis of firing pattern and input resistance, DG granule cells could be divided into two distinct categories, termed type 1 and type 2 according to Nenov et al. (2015). When comparing type 1 *vs* type 2 DG granule cells according to the genotype, we found that WT type 1 DG cells had a high R_{in} (368 ± 20 MΩ, $n = 13$) whereas WT type 2 DG cells had a significant lower R_{in} (279 ± 19 MΩ, $n = 16$, ** $p < 0.01$) (Table 2). For APP/PS1 mice, type 1 DG cells had a R_{in} of 368 ± 16 MΩ ($n = 17$) and type 2 DG cells a R_{in} of 294 ± 18 MΩ ($n = 14$, ** $p < 0.01$) (Table 2) but type 1 and type 2 R_{in} were not significantly different with respect to the genotype ($p = 0.993$ and $p = 0.562$ respectively) (Table 2). Type 1 DG granule cells exhibited spikes starting from a moderate intensity of stimulation (50–60 pA), increasing in frequency following steps increments (Fig. 3A). At current steps of high intensity (>120 pA), type 1 DG granule cells displayed spike frequency adaptation (Benda and Herz, 2003) as shown by the gradual decrease in the amplitude of APs leading to their complete block before the end of the current step (Fig. 3A). In contrast, type 2 DG granule cells fired throughout all the current step without failure (Fig. 3A) and exhibited firing frequencies that were linearly proportional to the intensity of the current step, *i.e.* the maximum number of APs was always observed for the highest current intensity (Fig. 3B). The proportion of type 1 *vs* type 2 DG granule cells was similarly distributed (WT: 46.7% *vs* 53.3% respectively, $n = 30$; APP/PS1: 54.8% *vs* 45.2% respectively, $n = 31$) and was not genotype-dependent ($p = 0.366$, Chi-square = 0.815, Chi-squared test). Regardless of current step intensity, APP/PS1 DG granule cells fired significantly more spikes that WT DG granule cells for both type 1 and type 2 (Fig. 3B; type 1: F = 38.44, DF = 1, *** $p < 0.0001$; type 2: F = 47.25, DF = 1, *** $p < 0.0001$, two way ANOVA). Moreover, regardless of type, the interspike interval was shorter for APP/PS1 DG granule cells than WT DG granule cells highlighting the higher excitability of APP/PS1 DG granule cells (Fig. 3C; type 1: F = 25.37, DF = 1, *** $p < 0.0001$; type 2: F = 15.53, DF = 1, *** $p < 0.0001$, two way ANOVA). In order to investigate spike frequency adaptation, *i.e.* the reduction of the firing rate for a stimulus of constant intensity, we examined the last three interspike intervals in type 2 DG granule cells to search for possible differences between WT and APP/PS1 mice. Regardless of the interval, *i.e.* the third, the second or the first, they were no differences between genotypes (data not shown). Therefore, APP/PS1 type 1 and type 2 DG granule cells spiked at a higher frequency compared to WT in response to current

Table 1
Comparison between action potentials properties in DG granule cells from WT and APP/PS1 female mice. Data are mean ± SEM. Values between brackets are *n* values. *p* values were obtained with Student's *t*-test (amplitude: $p = 0.070$; overshoot: $p = 0.064$; peak time: $p = 0.885$; RMP: * $p < 0.05$; AP threshold: $p = 0.764$; I_{thr}: *** $p < 0.001$; t_{50}: $p = 0.848$; R_{in}: $p = 0.552$). RMP: resting membrane potential. t_{50}: time to get half amplitude of AP. R_{in}: input resistance.

	Amplitude (mV)	Overshoot (mV)	Peak time (ms)	RMP (mV)	AP threshold (mV)	I_{thr} (pA)	t_{50} (ms)	R_{in} (MΩ)
WT	132.2 ± 2.1 (12)	62.5 ± 2.1 (12)	2.4 ± 0.1 (12)	−72.7 ± 0.9 (23)	−33.2 ± 2.7 (10)	56 ± 3.7 (30)	1.76 ± 0.09 (12)	323 ± 15 (32)
APP/PS1	125.4 ± 2.8 (13)	55.7 ± 2.7 (13)	2.4 ± 0.1 (13)	−75.4 ± 0.7 (15)	−32.1 ± 2.2 (10)	40.3 ± 2 (31)	1.74 ± 0.09 (13)	335 ± 14 (31)

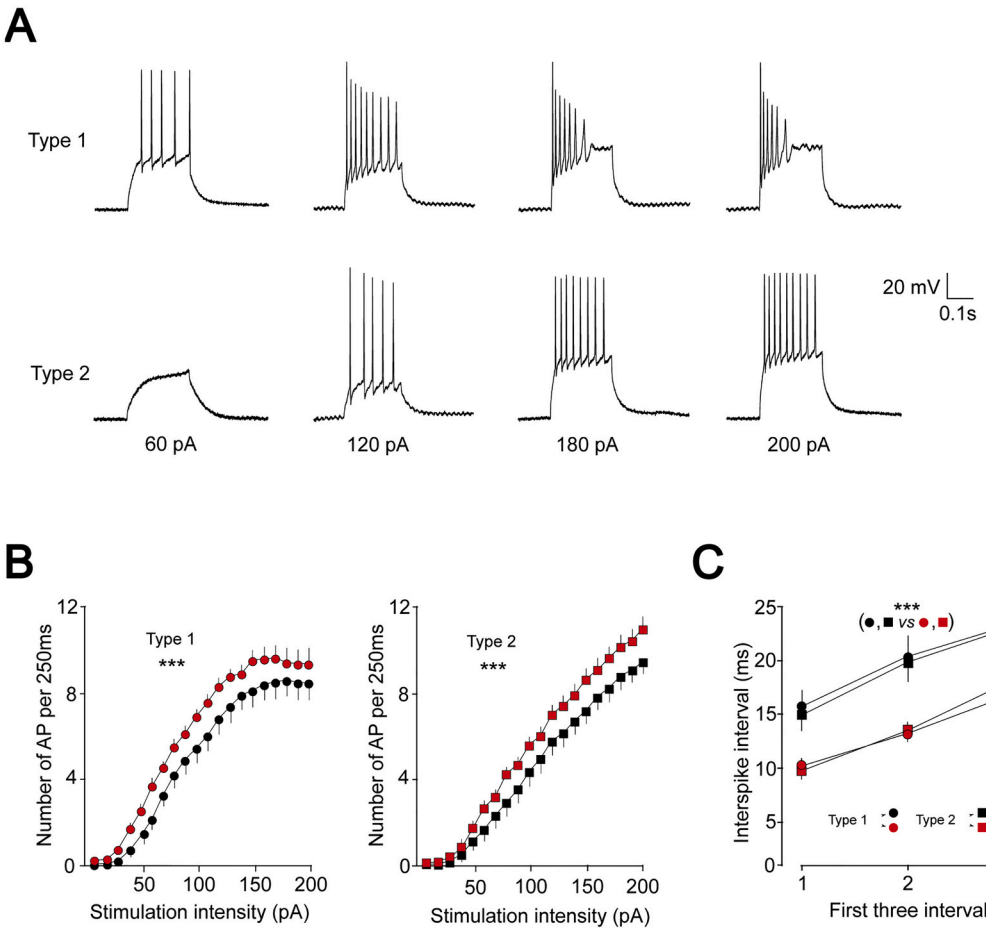

Fig. 3. APP/PS1 DG granule cells display higher excitability than WT. A. Representative trains of APs elicited by long depolarizing current steps (250 ms) of increasing intensity in WT DG granule cells. Cells were recorded from a membrane potential close to −70 mV in the whole-cell configuration of the patch clamp technique. DG granule cells were sorted into type 1 and type 2 cells according to their firing patterns. Whatever the genotype, type 1 and type 2 cells were similarly distributed (Type 1: WT = 45.1%, $n = 14$, APP/PS1 = 54.9%, $n = 17$; Type 2: WT = 53.3%, $n = 16$, APP/PS1 = 46.7%, $n = 14$; $p = 0.366$, 1-proportion Z test). B. Input-output curves for type 1 and type 2 DG granule cells. The number of spikes elicited in response to 250 ms-long depolarizing current steps with 10 pA increments was significantly higher in APP/PS1 *vs* WT DG cells for both type 1 and type 2 (type 1: WT, black circles; APP/PS1, red circles, F = 38.44, DF = 1, *** $p < 0.0001$, 2 way ANOVA; type 2: WT, black squares, APP/PS1, red squares, F = 47.25, DF = 1, *** $p < 0.0001$, 2 way ANOVA). Whatever the genotype the number of spikes elicited in response to 250 ms-long depolarizing current steps with 10 pA increments increased linearly for type 2 but reached a plateau for type 1. C. Interspike interval (ISI) plotted as a function of the first three intervals for a 180 pA pulse (first spike interval type 1: WT: 15.5 ± 1.6 ms, $n = 13$; APP/PS1: 10.4 ± 0.8, $n = 17$, ** $p < 0.01$; first spike interval type 2: WT: 14.6 ± 1.4 ms, $n = 17$; APP/PS1: 9.6 ± 0.7, $n = 14$, ** $p < 0.01$) (second spike interval type 1: WT: 20.1 ± 1.9 ms, $n = 13$; APP/PS1: 13.3 ± 1, $n = 17$, ** $p < 0.01$; second spike interval type 2: WT: 19.6 ± 1.9 ms, $n = 17$; APP/PS1: 13.5 ± 1.2 ms, $n = 14$, * $p = 0.05$) (third spike interval type 1: WT: 23.2 ± 2.1 ms, $n = 13$; APP/PS1: 17.1 ± 1.5, $n = 16$, * $p < 0.05$; third spike interval type 2: WT: 23.1 ± 1.3 ms, $n = 17$; APP/PS1: 18.2 ± 1.9, $n = 14$, $p = 0.08$). Whatever the type, the first three ISI were significantly higher for WT mice compared to APP/PS1 mice (WT type 1 black circles, APP/PS1 type 1 black squares; F = 25.37, DF = 1, *** $p < 0.0001$; WT type 2 red circles, APP/PS1 type 2 red squares, F = 15.53, DF = 1, *** $p = 0.0002$, 2 way ANOVA).

steps.

3.4. The potentiation of population spike amplitude is impaired at the LPP-DG synapse in APP/PS1 mice

It has recently been reported that the excitability of DG granule cells was highly plastic but also remarkably modulated by the long-term potentiation of MPP-DG synaptic transmission (Lopez-Rojas et al., 2016). We first recorded input-output relationships by stimulating the LPP with increasing intensity (0–300 μA; 200 μs at 0.1 Hz). This range of stimuli triggered a population spike reflecting the generation of action potentials in DG granule cells in response to the synaptic stimulation of LPP inputs (Fig. 4A left panel). The population spike amplitude (PSA) plotted as a function of stimulus intensity was best fitted by a non-linear regression, which plateaued within 250–300 μA (Fig. 4A right panel). Input-output relationships were significantly different between genotypes (F = 26.11, DF = 1, *** $p < 0.0001$, two way ANOVA) with APP/PS1 mice at 6 months of age always exhibiting a smaller PSA compared to the aged-matched WT for a given stimulation intensity (Fig. 4A right panel). This indicated an alteration of spike transfer between the entorhinal cortex and DG granule cells in APP/PS1 female mice. As APP/PS1 DG granule cells displayed higher intrinsic excitability, an increase in

Table 2
Comparison of action potentials properties of type 1 and type 2 DG granule cells between WT and APP/PS1 female mice. Data are mean ± SEM. For the calculation of the 1ST AP latency, minimal current step intensity was about 54 pA for WT and 40 pA for APP/PS1. Fast and slow AHP were measured in current clamp mode using a 250 ms pulse duration. The fast AHP was measured as the amplitude between the AP threshold and the peak of its fast repolarization. The slow AHP was measured as the amplitude between the AP threshold and the amplitude at the end of the 250 ms pulse. Values between brackets are *n* values. *p* values were obtained with Student's *t*-test. ADP: after depolarisation. AHP: after hyperpolarisation. I_{thr}: AP current threshold (minimal current intensity inducing an AP).

	WT				APP/PS1			
	Type 1	*p* (1 *vs* 2)	Type 2	*p* Type 1 (WT *vs* APP/PS1)	Type 1	*p* (1 *vs* 2)	Type 2	*p* Type 2 (WT *vs* APP/PS1)
1st AP latency (ms)	160 ± 9.1 (13)	0.178	177.4 ± 8.5 (17)	0.809	163 ± 8.2 (17)	0.746	158.4 ± 12.1 (14)	0.198
ADP (mV)	8.2 ± 0.7 (13)	0.244	9.5 ± 0.8 (16)	0.217	9.4 ± 0.7 (17)	0.824	9.7 ± 0.8 (14)	0.897
Fast AHP (mV)	18 ± 0.9 (13)	0.086	15.3 ± 1.1 (17)	0.525	17.2 ± 0. 8(17)	0.018*	14.4 ± 0.8 (14)	0.561
Slow AHP (mV)	10.3 ± 1 (13)	0.209	8.6 ± 0.9 (16)	0.318	9.2 ± 0.7 (17)	0.343	8.2 ± 0.7 (12)	0.764
I_{thr} (pA)	53.1 ± 3.4 (13)	0.493	58.2 ± 5.9 (17)	0.001**	37.1 ± 2. 9(17)	0.078	43.6 ± 2.5 (14)*	0.042*
R_{in} (MΩ)	368 ± 20 (13)	0.003**	279 ± 19 (16)	0.993	368 ± 16 (17)	0.004**	294 ± 17 (14)	0.562

PSA may have been expected in APP/PS1 mice. The decreased PSA in APP/PS1 mice for a given stimulation intensity may be caused by decreased EPSC amplitude due to less excitable PP fibers through reduced release probability or less PP inputs. However, the mean amplitude of EPSCs (stimulus intensity range: 20–65 μA) was not significantly different between genotypes (WT: 150.8 ± 12.4 pA, $n = 30$; APP/PS1: 150.9 ± 14.3 pA, $n = 29$, $p = 0.997$).

We then tested whether spike transfer from the entorhinal cortex to the DG was modulated by a high frequency stimulation (HFS) protocol consisting of 3 bursts of 100 stimuli at 100 Hz with a 10 s interburst interval. HFS triggered a robust and long-lasting potentiation of PSA in WT female mice (187 ± 14%, $n = 17$). The potentiation of PSA was completely blocked by 50 μM AP-V ($n = 9$) (Fig. 4B) evidencing the requirement of NMDA receptors (Errington et al., 1987; Jester et al., 1995). The potentiation of PSA was significantly reduced by half in APP/PS1 mice (146 ± 8%, $n = 16$, * $p < 0.05$) (Fig. 4B). As the input/output relationships were significant different between genotypes (Fig. 4A), stimulating intensities triggering 30–35% of the maximal amplitude of PSA were not in a same range between WT and APP/PS1 (WT: 60–80 μA; APP/PS1: 70–90 μA). We therefore checked whether the degree of potentiation of PSA induced by the HFS protocol was related to the baseline amplitude of population spike (0.8–1.6 mV) triggered by stimuli intensities in the range 60–100 μA. Regardless of genotype, the degree of potentiation of PSA was not related to its baseline amplitude (goodness of fit: $R2_{WT} = 0.11$, $Sy.x_{WT} = 57.8$, $n = 17$; $R2_{APP/PS1} = 0.002$, $Sy.x_{APP/PS1} = 35.2$, $n = 33$).

Worthy of note, the strong potentiation of PSA induced by HFS occurred in the absence of significant alterations in synaptic strengh as shown by the lack of significant potentiation of EPSCs measured at 50–60 min *versus* the baseline (100%) for both genotype (Fig. 4C) (WT: 117 ± 12%, $n = 15$, $p = 0.18$; APP/PS1: 112 ± 9%, $n = 16$, $p = 0.21$). It is very unlikely this lack of potentiation was related to a "wash out" phenomenon that could occur during whole-cell patch clamp recordings as the same HFS protocol induced a significant increase in the EPSP amplitude/slope ratio in the following experiments (see Fig. 5D). An early potentiation of EPSCs following the application of HFS was observed for both genotypes, although not significantly different (10–20 min, WT: 156 ± 12%, $n = 16$; APP/PS1: 157 ± 10%, $n = 16$, $p = 0.98$). Therefore in our experimental conditions, the long term potentiation of PSA does not result from major changes in excitatory synaptic currents.

3.5. The excitability of DG granule cells is differently affected by high frequency stimulation in WT vs APP/PS1 mice

In order to gain information linking spike transfer at the LPP-DG synapse to DG granule cells excitability, we studied the coupling between EPSPs and the generation of spikes in whole-cell current clamp recordings. Fig. 5A (left panel) shows representative electrotonus and action potentials (APs) in a DG granule cell from a WT mouse in response to the stimulation of LPP by short (200 μs) depolarizing current steps (in 10 μA increments) in current-clamp mode at a membrane potential close to −70 mV.

The EPSP-to-Spike (E-S) curve, which relates EPSP-slopes to the associated AP firing probability, was generated by applying increasing stimuli to cover from a sub-threshold EPSP evoking no action potential to an EPSP evoking an action potential with 100% probability (Fig. 5B). EPSP slopes were measured during the first two milliseconds (Fig. 5A), a time window that mainly reflects the fast component of AMPA receptor mediated synaptic transmission (Lopez-Rojas et al., 2016). In control conditions, prior to the application of the HFS protocol, there were no significant differences between genotypes in the E-S curves ($p = 0.849$) (Fig. 5B, solid lines). We investigated whether the probability of discharge of postsynaptic DG granule cells in response to excitatory synaptic stimulation was differently affected in WT *vs* APP/PS1 mice. We compared E-S curves generated in the absence or after applying the HFS protocol triggering PSA potentiation. The HFS protocol induced a significant leftward shift of the E-S curves (Fig. 5B, dotted lines) in both genotypes (EC_{50} WT: 5.96 ± 0.38, $n = 15$, EC_{50} $WT_{after\ HFS}$: 4.51 ± 0.41, $n = 11$, * $p < 0.05$; EC_{50} APP/PS1: 5.85 ± 0.39, $n = 15$, EC_{50} $APP/PS1_{after\ HFS}$: 3.92 ± 0.27, $n = 10$, ** $p < 0.01$) (Fig. 5C). Remarkably, this leftward shift was significantly larger for APP/PS1 *vs* WT mice ($F = 489.9$, $DF = 1$, *** $p < 0.001$, 2 way ANOVA), corresponding to a higher increase in E-S coupling following the HFS protocol. E-S potentiation corresponds to the strengthening of the electrical coupling between the dendritic synaptic inputs and the soma, which results in greater action potential output for a given synaptic input. It is known to depend on the intrinsic leakiness of dendritic and somatic compartments but also on synaptic inhibition due to GABA-A receptors. As all experiments were performed in the presence of bicuculline, any change in the E-S potentiation would likely be related to a change in synaptically driven depolarization and propagation to the spike trigger zone within the soma. The leftward shift indicates an increased excitability in DG granule cells induced by HFS, *i.e.* to a given EPSP slope corresponds a higher AP firing probability. These results show that HFS induces long lasting changes in the intrinsic properties of DG granule cells, likely related to dendritic properties, with a more pronounced effect for APP/PS1 genotype.

While the coupling EPSP slope - AP firing probability is increased in APP/PS1 mice following HFS, the level of PSA potentiation is lower in APP/PS1 mice than in WT mice. A possible explanation for these puzzling results could come from the decreased stimulation - PSA relationship in APP/PS1 mice (Fig. 5A), which makes the HFS induction

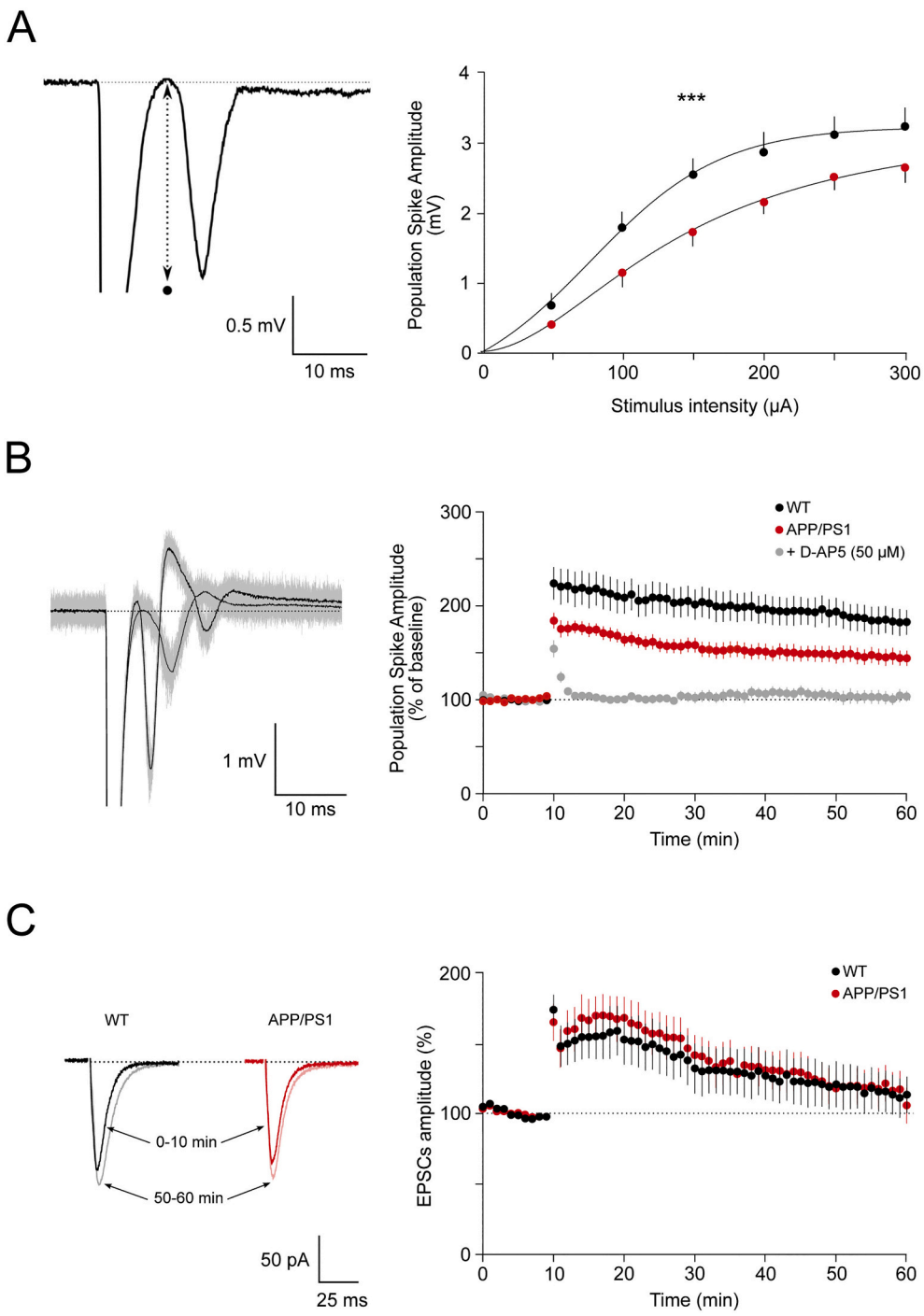

Fig. 4. Transfert of information at the LPP-DG synapse is altered in APP/PS1 female mice. A. Left panel shows representative traces of population spike in DG granule cells from a WT mouse. The double arrows dotted line represents the amplitude of the population spike. Right panel shows input-output relationship between the population spike amplitude and the stimulus intensity. For each intensity, WT (black circles) and APP/PS1 (red circles) relationships were significantly different (50 μA: WT = 0.68 ± 0.12, APP/PS1 = 0.40 ± 0.07; 100 μA: WT = 1.79 ± 0.19, APP/PS1 = 1.14 ± 0.10; 150 μA: WT = 2.54 ± 0.22, APP/PS1 = 1.71 ± 0.17; 200 μA: WT = 2.85 ± 0.26, APP/PS1 = 2.14 ± 0.16; 250 μA: WT = 3.10 ± 0.25, APP/PS1 = 2.50 ± 0.17; 300 μA: WT = 3.20 ± 0.27, APP/PS1 = 2.62 ± 0.18, F:26.11, DF:1, *** $p < 0.0001$, 2 way ANOVA). Both genotypes were best fitted by a non-linear regression. The goodness-of-fit was assessed by the coefficient of determination R2 ($R2_{WT} = 0.998$; $R2_{APP/PS1} = 0.852$). B. Left panel shows representative traces of population spike before (white circle) and after HFS (black circle) in DG granule cells. Population spike amplitude were recorded from a membrane potential close to −70 mV in the presence of bicuculline (10 μM). The potentiation of population spike was induced by 3 bursts of 100 stimuli at 100 Hz with a 10-s interburst interval (HFS). Light grey traces are individual traces and black traces are the averaged traces of 60 sweeps before and after HFS. Right panel shows the time course of potentiation of population spike (WT: black circles, APP/PS1:red circles). The average of normalized population spike amplitude (PSA) between 50 and 60 min after HFS protocol showed a significant reduction in APP/PS1 female mice (WT: 187 ± 14%, $n = 17$; APP/PS1: 146 ± 8%, $n = 16$; * $p < 0.05$, *t*-test). The potentiation was completely blocked by AP-V (50 μM, light grey circles) ($n = 9$). C. Left panel shows representative averaged EPSCs recorded from a holding potential of −70 mV in voltage-clamp during the baseline (0–10 min) and after (50–60 min) HFS in DG granule cells from WT and APP/PS1 mice. Right panel shows representative time course of EPSCs before and after HFS in WT and APP/PS1. Note the lack of significant long-term potentiation of EPSCs at 50–60 min whatever the genotype (WT: 117 ± 12%, $n = 15$, $p = 0.18$; APP/PS1: 112 ± 9%, $n = 16$, $p = 0.21$). All experiments were done in the presence of bicuculline (10 μM).

protocol less efficient to promote potentiation of PSA in APP/PS1 mice. Since the slope of EPSPs determines to some extent the amplitude of population spike, we considered the values of the slope before and after HFS for both genoypes. Within the stimulus intensity range of 20–40 μA, EPSPs slope was not significantly different for WT ($WT_{before\ HFS}$: 3.24 ± 0.35 mV/ms, $n = 10$; $WT_{after\ HFS}$: 3.40 ± 0.37 mV/ms, $n = 17$, $p = 0.772$) whether it was significantly decreased in APP/PS1 following HFS ($APP/PS1_{before\ HFS}$: 4.33 ± 0.52 mV/ms, $n = 12$; $APP/PS1_{after\ HFS}$: 2.90 ± 0.42 mV/ms, $n = 12$, * $p = 0.0458$). Therefore, although APP/PS1 DG granule cells are more excitable, *i.e.* able to fire more APs in response to a given synaptic input (EPSPs), the HFS induction protocol was not effective in potentiating EPSPs slope.

We then looked at the ratio between the EPSP amplitude and the EPSP slope for subthreshold EPSPs (*i.e.* not triggering APs) before and after HFS. Whereas EPSP slopes concern synaptic transmission, EPSP amplitudes are strongly determined by dendritic integration due to voltage-dependent ionic channels (Lopez-Rojas et al., 2016). We found a significant increase in the EPSP amplitude/slope ratio for APP/PS1 mice ($APP/PS1_{before\ HFS}$: 4.55 ± 0.18, $n = 15$; $APP/PS1_{after\ HFS}$: 6.08 ± 0.31, $n = 11$, *** $p < 0.001$) but not for WT mice ($WT_{before\ HFS}$: 4.9 ± 0.3, $n = 15$;

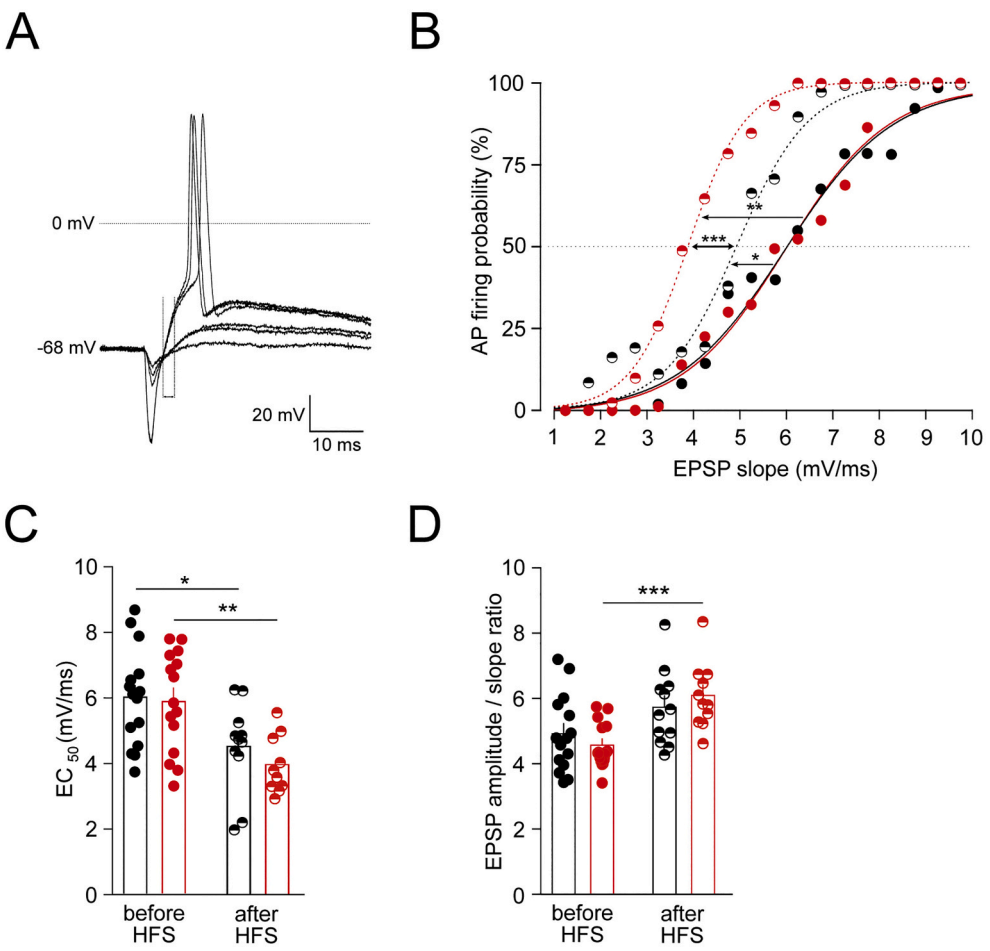

Fig. 5. Plasticity of itrinsic excitability in DG granule cells. A. Representative action potentials (APs) elicited in response to 200 μs depolarizing current steps with 10 μA increments in a DG granule cell from WT mouse. The DG granule cell was recorded from a membrane potential close to −70 mV in the whole-cell configuration of the patch clamp technique. B. E-S curves before and after high frequency stimulation (HFS). For each genotype (WT, black circles; APP/PS1, red circles) EPSP-slope values were calculated for the first two milliseconds and plotted *versus* the probability to fire action potentials. EPSP slope value giving a spike probability of 50% were graphically determined from the sigmoidal curves. In the absence of HFS, E-S curves were similar for both genotype (WT: 5.97, Hill slope = 0,37, $n = 15$; APP/PS1: 5.98, Hill slope = 0.39, $n = 15$). HFS induced prominent shifts of E-S curves to the left (WT:4.98, $n = 11$, F = 661.8, DF = 1, *** $p < 0.0001$, 2 way ANOVA; APP/PS1:3.88, $n = 10$, F = 724.9, DF = 1, *** $p < 0.0001$, 2 way ANOVA), which were significant for both genotype (WT: −1.45 ± 0.57 mV/ms, * $p = 0.018$; APP/PS1: −1.93 ± 0.53 mV/ms, ** $p = 0.0014$) but larger for APP/S1 *vs* WT (F = 489.9, DF = 1, *** $p < 0.0001$, 2 way ANOVA). C. A significant shift of EC_{50} in the E-S relation was induced by HFS for both WT (WT: 5.96 ± 0.38, $n = 15$, $WT_{after\ HFS}$: 4.51 ± 0.41, $n = 11$, * $p < 0.05$) and APP/PS1 (APP/PS1: 5.85 ± 0.39, $n = 15$, $APP/PS1_{after\ HFS}$: 3.92 ± 0.27, $n = 10$, ** $p < 0.01$) although with a larger amplitude for the APP/PS1 genotype. D. EPSP amplitude/slope ratio before and after synaptic potentiation induced by HFS. The amplitude/slope ratio was not different between WT and APP/PS1 mice before (WT: 4.90 ± 0.30, $n = 15$; APP/PS1: 4.55 ± 0.18, $n = 15$, $p = 0.332$) or after synaptic potentiation induced by HFS ($WT_{after\ HFS}$: 5.72 ± 0.33, $n = 11$; $APP/PS1_{after\ HFS}$: 6.08 ± 0.31, $n = 10$, $p = 0.406$) whereas it was significantly increased by HFS in APP/PS1 mice (APP/PS1: 4.55 ± 0.18, $n = 15$; $APP/PS1_{after\ HFS}$: 6.08 ± 0.31, $n = 10$, *** $p < 0.001$) but not for WT (WT: 4.90 ± 0.30, $n = 15$; $WT_{after\ HFS}$: 5.72 ± 0.33, $n = 11$, $p = 0.088$).

$WT_{after\ HFS}$: 5.7 ± 0.33, $n = 12$, $p = 0.08$) (Fig. 5D).

4. Discussion

In the present study we investigated the electrophysiological properties of DG granule cells under conditions of robust Aβ plaque loading and unambiguous neuroinflammatory activation of astrocytes and microglia in APP/PS1 female mice. These molecular and cellular alterations are concomitant with functional deficits in hippocampus-dependent memory tasks. We report prominent differences in the intrinsic excitability of DG granule cells and in the plasticity of E-S coupling leading to dysfunctional spike transfer between the entorhinal cortex and the hippocampus.

4.1. Histopathological and behavioral alterations in APP/PS1 female mice

We report that APP/PS1 female mice at 6 months of age displayed Aβ plaques and expressed abundant hypertrophic astrocytes and amoeboïd microglia preferentially located in the *stratum moleculare* of the DG, a region early affected in the spatio-temporal progression of the disease (Hurtado et al., 2010). Our results extend those of Richetin et al. (2017) who reported in older APP/PS1 female mice (7–9 months) the presence of abundant hypertrophic astrocytes in the DG. Concomitantly, APP/PS1 female mice displayed impaired contextual fear conditioning and object location task, two hippocampus-dependent memory tasks. These results are in general agreement with other studies reporting impairments of CFC in APP/PS1 mice as early as 4–6 months of age (Kilgore et al., 2010; Bonardi et al., 2011; Janus et al., 2015) and OLT in APP/PS1 female mice of 7–9 months of age (Richetin et al., 2017). Regardless of the age, APP/PS1 mice in our study were not significantly more active than the aged-matched WT. However, at 6 months of age, although not significant, our results show a trend, which could indicate slightly more active APP/PS1 mice. It should be noted that we did not assess progression of CFC at 9 months of age because the deficits in APP/PS1 female mice at 8 and 13 months of age, are similar to those in 6 month old mice (Janus et al., 2015). Differences in mice gender and in training protocols such as foot shock intensity and/or its duration prevented a closer and more relevant comparison of our results with those of all these previous studies.

4.2. Passive and active membrane properties of WT and APP/PS1 DG granule cells

We observed a slight increase in the resting membrane potential (RMP) in APP/PS1 DG granule cells compared to WT mice (by about 2.5 mV). This is in clear contrast to the finding of Minkeviciene et al. (2009) who reported a decreased RMP (by about 15 mV) in DG granule cells following the exogenous application of fibrillar $A\beta_{1-42}$ in WT slices (Minkeviciene et al., 2009). We do not have a firm explanation for this discrepancy, but we would like to point out that under no circumstances can an exogenous application of fibrillar $A\beta_{1-42}$ on a WT slice be considered similar to an APP/PS1 slice in either time or space. Furthermore, the mean RMP reported for DG granule cells from WT mice by Minkeviciene et al. (2009) was exceptionally hyperpolarized (close to −91 mV).

Adult DG granule cells are constituted of newly generated granule cells (immature granule cells) and mature granule cells. These two populations can be divided into type 1 and type 2, on the basis of their input resistance and firing pattern. Type 1 DG granule cells are considered to be young/immature neurons whereas type 2 DG granule cells would correspond to more mature neurons (van Praag et al., 2002; Mongiat et al., 2009; Spampanato et al., 2012). We found a ratio of about 50 to 50% of type 1 *vs* type 2 DG granule cells in WT DG granule cells. This unexpected result showing a number of type 1 DG granule cells (presumably less mature) almost similar to the number of type 2 DG granule cells (presumably more mature) deserves further investigations since the majority of granule neurons at 6 months old are presumably mature. Worthy of note, a ratio shifted towards even less type 2 (70 to 30% of type 1 *vs* type 2 DG granule cells) has been reported in 9 months old WT mice (Nenov et al., 2015). Contrary to Nenov et al. (2015), we report that the ratio between type 1 and type 2 DG granule cells was not significantly affected by the genotype while it was unbalanced (60 to 40% of type 1 *vs* type 2 DG granule cells) for 9 months old Tg2576 mice (Nenov et al., 2015). In addition, we did not observe any genotype-related differences in R_{in} while Nenov et al. (2015) reported a significant difference for type 2 DG granule cells between WT and Tg2576 mice. These differences could be related to different experimental conditions. Firstly, the transgenic mouse model was different (Tg2576 *vs* APP/PS1). Second, we used only female mice whereas male and female were used indifferently in Nenov's study introducing an experimental gender bias. Finally, we studied 6 months old female mice whereas 9 months old male and female mice were used in Nenov's study. Interestingly, Nenov et al. (2015) suggested that the differences observed in WT *vs* Tg2576 DG granule cells could be due to a decrease in proliferation, survival, maturation or integration of newborn DG neurons within DG. If it holds, the younger age of our mice could blunt differences due to these mechanisms. It should be noted that the estrous cycle is known to alter hippocampal spinogenesis and spine densities (Gould et al., 1990; Hara et al., 2015) and adult-born DG cells in APP/PS1 female mice at older age than in our study display impaired dendritic spine density contributing to reduced survival rate (Richetin et al., 2017). We clearly show that the population spike amplitude, which is related to the number of DG granule cells discharging, was decreased in APP/PS1 *vs* WT at a given stimulation intensity. In contrast, the intrinsic excitability of DG granule cells was significantly increased in APP/PS1 *vs* WT. Consistent with these data, the current threshold (I_{thr}) to trigger APs was significantly lower in APP/PS1 *vs* WT for both type 1 and type 2 DG granule cells. The potential mechanisms underlying the increased excitability in APP/PS1 DG granule cells may involve voltage-dependent channels such as A-type K^+ channels (Sun et al., 2011) and calcium-activated K^+ channels (Brenner et al., 2005; Ye et al., 2010).

4.3. Plasticity of spike transfer and intrinsic excitability in DG granule cells of WT vs APP/PS1

Synaptic and non-synaptic, *i.e.* intrinsic excitability, forms of plasticity likely coexist and interact coherently to regulate information processing in the brain (Daoudal and Debanne, 2003). Since both types of DG granule cells likely participate to the transfert of information at the PP-DG synapse and since immature DG granule cells display similar dendritic complexity than mature granule cells (Morgenstern et al., 2008), we analysed the pathophysiological modulation of the transfert of information at the LPP-DG synapse considering DG granule cells as a whole. We provide strong evidence that plasticity of intrinsic excitability of DG granule cells controls spike transfer at the LPP-DG synapse and is affected in APP/PS1 mice. This plasticity has a lower induction-threshold than the archetypal synaptic plasticity described in DG mature granule cells (Lopez-Rojas et al., 2016) and likely accounts for a large part of the partial impairment of the potentiation of PSA following HFS. Indeed, HFS triggered strong potentiation of PSA in DG granule cells unrelated to enhanced synaptic plasticity even though this potentiation requires the activation of NMDA receptors activated by ambiant glutamate (Errington et al., 1987; Sah et al., 1989) and likely modulating dendritic integration properties (Krueppel et al., 2011).

In the present work, we report that the potentiation of PSA following the HFS-induction protocol was impaired in APP/PS1 mice. Interestingly, the exogenous application of soluble Aβ oligomers lead to the impairment of the HFS-induced potentiation of PSA in the adjacent *stratum pyramidale* of CA1 neurons in mouse hippocampal slices (Lei et al., 2016). The authors attributed this impairment to reduced extracellular glutamate uptake, which resulted in an increase in ambiant glutamate and consequently an increase in NMDA receptor-dependent neuronal excitability. However, the exogenous application of soluble Aβ oligomers does not replicate either in time (acute bolus of soluble Aβ oligomers *in vitro versus* progressive increase in soluble Aβ oligomers concentration *in vivo*) or space (homogenous soluble Aβ oligomers concentration within all the slice *in vitro versus* localized soluble Aβ oligomers concentration increase in the vicinity of Aβ plaques *in vivo*) what occurs *in vivo* making any meaningful comparison difficult. Furthermore the cellular origin of Aβ oligomers (neurons *vs* glia) is not considered in exogenous application.

Although the potentiation of PSA following HFS is decreased in APP/PS1 mice as compared to WT mice, our results reveal that HFS increases the *E-S* coupling to a larger extent in APP/PS1 mice. Therefore while the intrinsic excitability of DG granule cells is increased the potentiation of PSA is decreased. This counter-intuitive result could be the result of a less efficient HFS protocol in APP/PS1 to induce potentiation of EPSPs. Indeed, our results show a significant decrease of EPSP potentiation after HFS in APP/PS1 leading to a decrease of PSA potentiation. EPSP amplitude is strongly determined by dendritic integration *via* voltage-dependent ionic channels therefore changes in dendritic processing of synaptic input could account for excitability changes. Therefore the increase of EPSP amplitude/slope ratio observed for APP/PS1 mice following HFS, but not for WT mice is likely related to the higher excitability of APP/PS1 DG granule cells but much less to variation in synaptic transmission. In good agreement with a major role of dendritic integration in intrinsic excitability of DG granule cells, the blockade of dendritic A-type potassium channels by 4-aminopyridine significantly increased the EPSP amplitude/slope ratio and decreased EC_{50} value (Lopez-Rojas et al., 2016). Consistent with a significant role of dendritic A-type potassium channels in a mouse model of AD, the observed dendritic depletion of Kv4.2, the potassium channel subunit, mediates the majority of A-type current, induces dendritic hyperexcitability in the CA1 region in hAPP mice (Hall et al., 2015).

The E-S coupling following HFS is remarkably different between WT and APP/PS1 mice. Therefore not only the increased intrinsic excitability but also a strengthened E-S coupling likely enhance spike transfer between the entorhinal cortex and the DG, which could participate in the well known enhanced excitability of hippocampal circuits in the AD pathology. This enhanced spike transfer could act as compensatory mechanisms for the well established early loss of perforant path fibers from the layer II of entorhinal cortex to the hippocampus encountered in

the course of the pathology (Llorens-Martín et al., 2014).

Worthy of note, the present study focused on the excitatory synaptic drive but it is questionable how this could relate to the *in vivo* situation with intact inhibitory drive. GABAergic interneurons in the DG are multiple and densely expressed in the hilus (for review, see Houser, 2007). Hilar interneurons project to perisomatic and proximal dendritic regions of DG granule cells (Amaral et al., 2007) exerting synaptic inhibition that shunts AP generation (Ben-Ari et al., 2005). While GABA-A receptors expressed by DG granule cells are responsible for a tonic inhibition (Engin et al., 2015) leading to their sparse activation, the activation of GABA-B receptors enhances DG granule cell activity by reducing synaptic inhibition driven by hilar interneurons (Burgard and Sarvey, 1991; Mott and Lewis, 1991; Mott et al., 1993; Foster et al., 2013). Interestingly it was recently reported that exogenous application of recombinant sAPP**α** in cultured hippocampal neurons reduced the probability of GABAergic synaptic vesicles release in a GABA-B R1a-dependent manner (Rice et al., 2019). At the PP-DG synapse, GABA-B R1a decrease GABAergic inhibition on proximal dendrites (Ben-Ari et al., 2005) and thus lead to increased DG cells output (Foster et al., 2013). In the APP/PS1 mouse model, a reduction in the rate of APP processing by α-secretase and an increase in the rate of APP cleavage by β-secretase lead to an increase in the sAPP**β**/sAPP**α** ratio (Tambini et al., 2019). Therefore, in the event of a significant effect of sAPP**β** on GABA-B R1a (yet to be studied) this could modulate PP-DG synapse activity. However due to the expression at the PP-DG synapse of different GABA-B receptors subtype, *i.e.* GABA-B R1a and GABA-B R1b, the control of the transfer of information at the perforant path to the hippocampus by GABAergic control of DG granule cells is a complex issue that clearly deserves further investigation.

In conclusion, our study report for the first time that a non-synaptic form of plasticity, *i.e.* the plasticity of intrinsic excitability of DG granule cells, is markedly impacted in a mouse model of AD. This is of paramount importance given the crucial role of the functional integrity of the DG in the formation of new memories, which is particularly impacted in AD. Thus in addition to expanding fundamental knowledge of AD, our results may open new avenues for improvement and/or therapeutic intervention.

Funding

This work was supported by a joint program between the University of Bordeaux and the China Scholarship Council (CSC) to NJ (Grant: 201506890031).

Declaration of Competing Interest

None declared.

Acknowledgments

We deeply thank Jeffrey Lopez-Rojas for his invaluable help with electrophysiological recordings, extremely fruitful discussions and constant availability and kindness. We thank Gaël Barthet for his constant support and very fruitful comments. We thank Benoit Silvestre de Ferron for the cartoon shown in Fig. 2. We thank the Bordeaux Imaging Center, part of the France Bioimaging national infrastructure ANR-10-INBS-04. We thank Patrice Mascalchi from the Bordeaux Imaging Center part of the France Bioimaging national infrastructure ANR-10-INBS-04 for his excellent technical support.

References

Aimone, J.B., Deng, W., Gage, F.H., 2011. Resolving new memories: a critical look at the dentate gyrus, adult neurogenesis and pattern separation. Neuron 70, 589–596.
Akiyama, H., Arai, T., Kondo, H., Tanno, E., Haga, C., Ikeda, K., 2000. Cell mediators of inflammation in the Alzheimer disease brain. Alzheimer Dis. Assoc. Disord. 14, 47–53.
Alzheimer's Association Report, 2018. Alzheimer's disease fact and figures. Alzheimers Dement. 14, 367–429.
Amaral, D.G., Scharfman, H.E., Lavenex, P., 2007. The dentate gyrus: fundamental neuroanatomical organization (dentate gyrus for dummies). Prog. Brain Res. 163, 3–22.
Bannerman, D.M., Sprengel, R., Sanderson, D.J., McHugh, S.B., Rawlins, J.N., Monyer, H., Seeburg, P.H., 2014. Hippocampal synaptic plasticity, spatial memory and anxiety. Nat. Rev. Neurosci. 15 (3), 181–192.
Barnes, L.L., Wilson, R.S., Bienias, J.L., Schneider, J.A., Evans, D.A., Bennett, D.A., 2005. Sex differences in the clinical manifestations of Alzheimer disease pathology. Arch. Gen. Psychiatry 62, 685–691.
Ben-Ari, Y., Cossart, R., Bernard, C., 2005. Multiple facets of GABAergic neurons and synapses: multiple fates of GABA signalling in epilepsies. Trends Neurosci. 28, 108–115.
Benda, J., Herz, A.V.M., 2003. A universal model for spike-frequency adaptation. Neural Comput. 15 (11), 2523–2564.
Bonardi, C., de Pulford, F., Jennings, D., Pardon, M.C., 2011. A detailed analysis of the early context extinction deficits seen in APPswe/PS1dE9 female mice and their relevance to preclinical Alzheimer's disease. Behav. Brain Res. 222 (1), 89–97.
Brenner, R., Chen, Q.H., Vilaythong, A., Toney, G.M., Noebels, J.L., Aldrich, R.W., 2005. BK channel beta4 subunit reduces dentate gyrus excitability and protects against temporal lobe seizures. Nat. Neurosci. 8, 1752–1759.
Burgard, E.C., Sarvey, J.M., 1991. Long-lasting potentiation and epileptiform activity produced by GABAB receptor activation in the dentate gyrus of rat hippocampal slice. J. Neurosci. 11 (5), 1198–1209.
Cès, A., Burg, T., Herbeaux, K., Héraud, C., Bott, J.B., Mensah-Nyagan, A.G., Mathis, C., 2018. Age-related vulnerability of pattern separation in C57BL/6J mice. Neurobiol. Aging 62, 120–129.
Colino, A., Malenka, R.C., 1993. Mechanisms underlying induction of long-term potentiation in rat medial and lateral perforant paths in vitro. J. Neurophysiol. 69 (4), 1150–1159.
Criscuolo, C., Fontebasso, V., Middei, S., Stazi, M., Ammassari-Teule, M., Yan, S.S., Origlia, N., 2017. Entorhinal cortex dysfunction can be rescued by inhibition of microglial RAGE in an Alzheimer's disease mouse model. Sci. Rep. 7, 42370.
Dahl, D., Sarvey, J.M., 1989. Norepinephrine induces pathway-specific long-lasting potentiation and depression in the hippocampal dentate gyrus. Proc. Natl. Acad. Sci. U. S. A. 86 (12), 4776–4780.
Daoudal, G., Debanne, D., 2003. Long-term plasticity of intrinsic excitability: learning rules and mechanisms. Learn. Mem. 10 (6), 456–465.
Deng, W., Aimone, J.B., Gage, F.H., 2010. New neurons and new memories: how does adult hippocampal neurogenesis affect learning and memory? Nat. Rev. Neurosci. 11, 339–350.
Engin, E., Zarnowska, E.D., Benke, D., Tsvetkov, E., Sigal, M., Keist, R., Bolshakov, V.Y., Pearce, R.A., Rudolph, U., 2015. Tonic inhibitory control of dentate Gyrus granule cells by α5-containing GABAA receptors reduces memory interference. J. Neurosci. 35 (40), 13698–13712.
Ennaceur, A., Neave, N., Aggleton, J.P., 1997. Spontaneous object recognition and object location memory in rats: the effects of lesions in the cingulate cortices, the medial prefrontal cortex, the cingulum bundle and the fornix. Exp. Brain Res. 113 (3), 509–519.
Errington, M.L., Lynch, M.A., Bliss, T.V., 1987. Long-term potentiation in the dentate gyrus: induction and increased glutamate release are blocked by D(−) aminophosphonovalerate. Neuroscience. 20 (1), 279–284.
Forner, S., Baglietto-Vargas, D., Martini, A.C., Trujillo-Estrada, L., LaFerla, F.M., 2017. Synaptic impairment in Alzheimer's disease: a Dysregulated symphony. Trends Neurosci. 40 (6), 347–357.
Foster, J.D., Kitchen, I., Bettler, B., Chen, Y., 2013. GABAB receptor subtypes differentially modulate synaptic inhibition in the dentate gyrus to enhance granule cell output. Br. J. Pharmacol. 168 (8), 1808–1819.
Gallagher, J.J., Minogue, A., Lynch, M., 2013. Impaired performance of female APP/PS1 mice in the Morris water maze is coupled with increased Aβ accumulation and microglial activation. Neurodegener. Dis. 11, 33–41.
Garcia-Alloza, M., Robbins, E.M., Zhang-Nunes, S.X., Purcell, S.M., Betensky, R.A., Raju, S., Prada, C., Greenberg, S.M., Bacskai, B.J., Frosch, M.P., 2006. Characterization of amyloid deposition in the APPswe/PS1ΔE9 mouse model of Alzheimer disease. Neurobiol. Dis. 24 (3), 516–524.
Gould, E., Woolley, C., Frankfurt, M., McEwen, B.S., 1990. Gonadal steroids regulate dendritic spine density in hippocampal pyramidal cells in adulthood. J. Neurosci. 10, 1286–1291.
Haettig, J., Stefanko, D.P., Multani, M.L., Figueroa, D.X., McQuown, S.C., Wood, M.A., 2011. HDAC inhibition modulates hippocampus dependent long-term memory for object location in a CBP-dependent manner. Learn. Mem. 18, 71–79.
Hall, A.M., Throesch, B.T., Buckingham, S.C., Markwardt, S.J., Peng, Y., Wang, Q., Hoffman, D.A., Roberson, E.D., 2015. Tau-dependent Kv4.2 depletion and dendritic hyperexcitability in a mouse model of Alzheimer's disease. J. Neurosci. 35, 6221–6230.
Hara, Y., Waters, E., McEwen, B., Morrison, J., 2015. Estrogen effects on cognitive and synaptic health over the lifecourse. Physiol. Rev. 95, 785–807.
Heneka, M.T., O'Banion, M., 2007. Inflammatory processes in Alzheimer's disease. J. Neuroimmunol. 184 (1–2), 69–91.
Heneka, M.T., Golenbock, D.T., Latz, E., 2015. Innate immunity in Alzheimer's disease. Nat. Immunol. 16, 229–236.
Houser, C.R., 2007. Interneurons of the dentate gyrus: an overview of cell types, terminal fields and neurochemical identity. Prog. Brain Res. 163, 217–232.

Hunsaker, M.R., Mooy, G.G., Swift, J.S., Kesner, R.P., 2007. Dissociations of the medial and lateral perforant path projections into dorsal DG, CA3, and CA1 for spatial and nonspatial (visual object) information processing. Behav. Neurosci. 121, 742–750.
Hurtado, D.E., Molina-Porcel, L., Iba, M., Aboagye, A.K., Paul, S.M., Trojanowski, J.Q., Lee, V.M., 2010. Aβ accelerates the spatiotemporal progression of tau pathology and augments tau amyloidosis in an Alzheimer mouse model. Am. J. Pathol. 177, 1977–1988.
Igarashi, K.M., Lu, L., Colgin, L.L., Moser, M.B., Moser, E.I., 2014. Coordination of entorhinal-hippocampal ensemble activity during associative learning. Nature. 510 (7503), 143–147.
Jankowsky, J.L., Fadale, D.J., Anderson, J., Xu, G.M., Gonzales, V., Jenkins, N.A., Copeland, N.G., Lee, M.K., Younkin, L.H., Wagner, S.L., Younkin, S.G., Borchelt, D. R., 2004. Mutant presenilins specifically elevate the levels of the 42 residue β-amyloid peptide in vivo: evidence for augmentation of a 42-specific γ secretase. Hum. Mol. Genet. 13, 159–170.
Janus, C., Flores, A.Y., Xu, G., Borchelt, D.R., 2015. Behavioral abnormalities in APPSwe/PS1dE9 mouse model of AD-like pathology: comparative analysis across multiple behavioral domains. Neurobiol. Aging 36 (9), 2519–2532.
Jester, J.M., Campbell, L.W., Sejnowski, T.J., 1995. Associative EPSP—spike potentiation induced by pairing orthodromic and antidromic stimulation in rat hippocampal slices. J. Physiol. Lond. 484, 689–705.
Kheirbek, M.A., Klemenhagen, K.C., Sahay, A., Hen, R., 2012. Neurogenesis and generalization: a new approach to stratify and treat anxiety disorders. Nat. Neurosci. 15 (12), 1613–1620.
Kilgore, M., Miller, C.A., Fass, D.M., Hennig, K.M., Haggarty, S.J., Sweatt, J.D., Rumbaugh, G., 2010. Inhibitors of class 1 histone deacetylases reverse contextual memory deficits in a mouse model of Alzheimer's disease. Neuropsychopharmacology. 35 (4), 870–880.
Krueppel, R., Remy, S., Beck, H., 2011. Dendritic integration in hippocampal dentate granule cells. Neuron 71 (3), 512–528.
Lei, M., Xu, H., Li, Z., Wang, Z., O'Malley, T.T., Zhang, D., Walsh, D.M., Xu, P., Selkoe, D. J., Li, S., 2016. Soluble Aβ oligomers impair hippocampal LTP by disrupting glutamatergic/GABAergic balance. Neurobiol. Dis. 85, 111–121.
Llorens-Martín, M., Blazquez-Llorca, L., Benavides-Piccione, R., Rabano, A., Hernandez, F., Avila, J., DeFelipe, J., 2014. Selective alterations of neurons and circuits related to early memory loss in Alzheimer's disease. Front. Neuroanat. 8 (38), 1–12.
Lopez-Rojas, J., Heine, M., Kreutz, M.R., 2016. Plasticity of intrinsic excitability in mature granule cells of the dentate gyrus. Sci. Rep. 6, 21615.
Marchetti, C., Marie, H., 2011. Hippocampal synaptic plasticity in Alzheimer's disease: what have we learned so far from transgenic models? Rev. Neurosci. 22, 373–402.
Mayer, M.L., Westbrook, G.L., Guthrie, P.B., 1984. Voltage-dependent block by Mg^{2+} of NMDA responses in spinal cord neurones. Nature 309, 261–263.
McNaughton, B.L., 1980. Evidence for two physiologically distinct perforant pathways to the fascia dentata. Brain Res. 199, 1–19.
Minkeviciene, R., Rheims, S., Dobszay, M.B., Zilberter, M., Hartikainen, J., Fülöp, L., Penke, B., Zilberter, Y., Harkany, T., Pitkänen, A., Tanila, H., 2009. Amyloid beta-induced neuronal hyperexcitability triggers progressive epilepsy. J. Neurosci. 29 (11), 3453–3462.
Mongiat, L.A., Espósito, M.S., Lombardi, G., Schinder, A.F., 2009. Reliable activation of immature neurons in the adult hippocampus. PLoS One 4 (4), e5320.
Morgenstern, N.A., Lombardi, G., Schinder, A.F., 2008. Newborn granule cells in the ageing dentate gyrus. J. Physiol. 586 (16), 3751–3757.
Mott, D.D., Lewis, D.V., 1991. Facilitation of the induction of long-term potentiation by GABAB receptors. Science. 252 (5013), 1718–1720.
Mott, D.D., Xie, C.W., Wilson, W.A., Swartzwelder, H.S., Lewis, D.V., 1993. GABAB autoreceptors mediate activity-dependent disinhibition and enhance signal transmission in the dentate gyrus. J. Neurophysiol. 69 (3), 674–691.
Mumby, D.G., Gaskin, S., Glenn, M.J., Schramek, T.E., Lehmann, H., 2002. Hippocampal damage and exploratory preferences in rats: memory for objects, places & contexts. Learn. Mem. 9, 49–57.
Nakashiba, T., Cushman, J.D., Pelkey, K.A., Renaudineau, S., Buhl, D.L., McHugh, T.J., Rodriguez Barrera, V., Chittajallu, R., Iwamoto, K.S., McBain, C.J., Fanselow, M.S., Tonegawa, S., 2012. Young dentate granule cells mediate pattern separation, whereas old granule cells facilitate pattern completion. Cell 149, 188–201.
Nenov, M.N., Tempia, F., Denner, L., Dineley, K.T., Laezza, F., 2015. Impaired firing properties of dentate granule neurons in an Alzheimer's disease animal model are rescued by PPARγ agonism. J. Neurophysiol. 113, 1712–1726.
Nimmerjahn, A., Kirchhoff, F., Helmchen, F., 2005. Resting microglial cells are highly dynamic Surveillants of brain parenchyma in vivo. Science. 308, 1314–1318.
Nowak, L., Bregestovski, P., Ascher, P., Herbet, A., Prochiantz, A., 1984. Magnesium gates glutamate-activated channels in mouse central neurones. Nature. 307, 462–465.
Penzes, P., Cahill, M.E., Jones, K.A., VanLeeuwen, J.E., Woolfrey, K.M., 2011. Dendritic spine pathology in neuropsychiatric disorders. Nat. Neurosci. 14 (3), 285–293.
Petersen, R.P., Moradpour, F., Eadie, B.D., Shin, J.D., Kannangara, T.S., Delaney, K.R., Christie, B.R., 2013. Electrophysiological identification of medial and lateral perforant path inputs to the dentate gyrus. Neuroscience 252, 154–168.
Phillips, R.G., LeDoux, J.E., 1992. Differential contribution of amygdala and hippocampus to cued and contextual fear conditioning. Behav. Neurosci. 106, 274–278.
Querfurth, H.W., LaFerla, F.M., 2010. Alzheimer's disease. N. Engl. J. Med. 362, 329–344.
Rice, H.C., de Malmazet, D., Schreurs, A., Frere, S., Van Molle, I., Volkov, A.N., Creemers, E., Vertkin, I., Nys, J., Ranaivoson, F.M., Comoletti, D., Savas, J.N., Remaut, H., Balschun, D., Wierda, K.D., Slutsky, I., Farrow, K., De Strooper, B., de Wit, J., 2019. Secreted amyloid-beta precursor protein functions as a GABA(B)R1a ligand to modulate synaptic transmission. Science. 363 (6423).
Richetin, K., Petsophonsakul, P., Roybon, L., Guiard, B.P., Rampon, C., 2017. Differential alteration of hippocampal function and plasticity in females and males of the APPxPS1 mouse model of Alzheimer's disease. Neurobiol. Aging 57, 220–231.
Sah, P., Hestrin, S., Nicoll, R.A., 1989. Tonic activation of NMDA receptors by ambient glutamate enhances excitability of neurons. Science 246, 815–818.
Sarlus, H., Heneka, M.T., 2017. Microglia in Alzheimer's disease. J. Clin. Invest. 127 (9), 3240–3249.
Schiweck, J., Eickholt, B.J., Murk, K., 2018. Important Shapeshifter: mechanisms allowing astrocytes to respond to the changing nervous system during development, injury and disease. Front. Cell. Neurosci. 12, 261.
Schmidt-Hieber, C., Jonas, P., Bischofberger, J., 2004. Enhanced synaptic plasticity in newly generated granule cells of the adult hippocampus. Nature 429 (6988), 184–187.
Selkoe, D.J., 2002. Alzheimer's disease is a synaptic failure. Science 298, 789–791.
Sinforiani, E., Citterio, A., Zucchella, C., Bono, G., Corbetta, S., Merlo, P., Mauri, M., 2010. Impact of gender differences on the outcome of Alzheimer's disease. Dement. Geriatr. Cogn. Disord. 30, 147–154.
Spampanato, J., Sullivan, R.K., Turpin, F.R., Bartlett, P.F., Sah, P., 2012. Properties of doublecortin expressing neurons in the adult mouse dentate gyrus. PLoS One 7, e41029.
Spires-Jones, T.L., Hyman, B.T., 2014. The intersection of amyloid beta and tau at synapses in Alzheimer's disease. Neuron 82, 756–771.
Stranahan, A.M., Mattson, M.P., 2010. Selective vulnerability of neurons in layer II of the entorhinal cortex during aging and Alzheimer's disease. Neural Plast. 2010, 108190.
Strange, B.A., Witter, M.P., Lein, E.S., Moser, E.I., 2014. Functional organization of the hippocampal longitudinal axis. Nat. Rev. Neurosci. 15 (10), 655–669.
Sun, W., Maffie, J.K., Lin, L., Petralia, R.S., Rudy, B., Hoffman, D.A., 2011. DPP6 establishes the A-type K^+ current gradient critical for the regulation of dendritic excitability in CA1 hippocampal neurons. Neuron 71, 1102–1115.
Tambini, M.D., Yao, W., D'Adamio, L., 2019. Facilitation of glutamate, but not GABA, release in familial Alzheimer's APP mutant Knock-in rats with increased β-cleavage of APP. Aging Cell 18 (6), e13033.
van Praag, H., Schinder, A.F., Christie, B.R., Toni, N., Palmer, T.D., Gage, F.H., 2002. Functional neurogenesis in the adult hippocampus. Nature 415, 1030–1034.
Wilhelmsson, U., Bushong, E.A., Price, D.L., Smarr, B.L., Phung, V., Terada, M., Ellisman, M.H., Pekny, M., 2006. Redefining the concept of reactive astrocytes as cells that remain within their unique domains upon reaction to injury. PNAS 103, 17513–17518.
Ye, H., Jalini, S., Mylvaganam, S., Carlen, P., 2010. Activation of large-conductance Ca^{2+} – Activated K^+ channels depresses basal synaptic transmission in the hippocampal CA1 area in APP (swe/ind) TgCRND8 mice. Neurobiol. Aging 31, 591–604.